

Time-Scale Coupling Between States and Parameters in Recurrent Neural Networks

Lorenzo Livi*

Abstract—We show that gating mechanisms in recurrent neural networks (RNNs) induce lag-dependent and direction-dependent effective learning rates, even when training uses a fixed, global step size. This behavior arises from a coupling between state-space time-scales (parametrized by the gates) and parameter-space dynamics during gradient descent. By deriving exact Jacobians for leaky-integrator and gated RNNs and applying a first-order expansion, we make explicit how constant, scalar, and multi-dimensional gates reshape gradient propagation, modulate effective step sizes, and introduce anisotropy in parameter updates. These findings reveal that gates act not only as filters of information flow, but also as data-driven preconditioners of optimization, with formal connections to learning-rate schedules, momentum, and adaptive methods such as Adam. Empirical simulations corroborate these predictions: across several sequence tasks, gates produce lag-dependent effective learning rates and concentrate gradient flow into low-dimensional subspaces, matching or exceeding the anisotropic structure induced by Adam. Notably, gating and optimizer-driven adaptivity shape complementary aspects of credit assignment: gates align state-space transport with loss-relevant directions, while optimizers rescale parameter-space updates. Overall, this work provides a unified dynamical systems perspective on how gating couples state evolution with parameter updates, clarifying why gated architectures achieve robust trainability in practice.

Index Terms—Recurrent neural networks; Dynamical systems; Gates; Time-scale coupling; Gradient descent.

I. INTRODUCTION

Training recurrent neural networks (RNNs) is typically analyzed from two largely separate perspectives. On the one hand, state-space dynamics emphasize how gating mechanisms stabilize hidden trajectories, regulate memory retention, and mitigate vanishing or exploding gradients. On the other hand, parameter-space dynamics emphasize the role of optimization algorithms—such as momentum or Adam—in adapting learning rates and reshaping update directions to ease training. Yet these two domains interact in ways that have not been made explicit.

Why do gated RNNs often train stably even with plain gradient descent? This robustness suggests that gates must influence not only the flow of information in state space, but also the dynamics of parameter updates. Yet the precise mechanisms by which state-space time-scales couple into optimization have remained implicit.

In this work, we show that gating mechanisms directly shape the dynamics of parameter updates. State-space time scales, parametrized by gates, determine the structure of Jacobian products in backpropagation through time. These

products, in turn, induce lag-dependent effective learning rates and directional anisotropy in parameter updates, even when the optimizer itself is non-adaptive. From this perspective, gates function as implicit, data-driven preconditioners of the optimization process, with formal connections to learning-rate schedules, momentum, and Adam—but here these behaviors emerge endogenously from gating rather than being externally imposed. Our contributions are:

- We show analytically that gates act as parametrized time scales that modulate lag-dependent effective learning rates. Our analysis introduces a perturbative expansion of Jacobian products, combining Fréchet derivative techniques with the structure of gated recurrent dynamics, making explicit how constant, scalar, and multi-gate RNNs modulate effective learning rates.
- We extend the theoretical analysis to directional effects, introducing the anisotropy index to quantify how gates shape the dominant subspaces of gradient propagation.
- We validate these predictions through targeted simulations on canonical tasks. Our results highlight that both gating and optimizer dynamics shape not only the magnitude but also the directional structure of temporal credit assignment, with task-dependent trade-offs.

The remainder of the paper is organized as follows. Section II reviews related work. Section III introduces the interpretation of gating mechanisms as parametrized time scales and formalizes the RNN models considered in our analysis. Section V develops the theoretical results linking state-space time scales with parameter dynamics, while Section VI discusses connections with classical optimization methods. Section VII presents empirical validations on canonical sequence tasks, and Section VIII concludes the paper. Supplementary material provides the derivation of the matrix-product expansion used in the analysis together with additional experimental figures.

II. RELATED WORKS

The study of RNNs has long been shaped by the well-known vanishing and exploding gradient problem [1], which affects the stability and learnability of long-term dependencies. While this issue traditionally focuses on the magnitude of gradients, recent work by Zucchet et al. [2] highlights a complementary phenomenon: as the memorization capacity of an RNN increases during training, the network output can become highly sensitive to small parameter variations. This heightened sensitivity arises even in the absence of vanishing or exploding gradients, suggesting that RNNs may undergo abrupt changes in behavior due to intrinsic instabilities in the learned parameter–state mapping. In a related vein, Ceni

*lorenz.livi@gmail.com

Lorenzo Livi is with the Open Institute of Technology, The Core, Triq Il-Wied Ta' L-Imsida, Msida, MSD 9021, Malta

[3] proposed Random Orthogonal Additive Filters, a class of architectures designed to stabilize and enrich recurrent dynamics via orthogonal transformations, mitigating instability without sacrificing representational power.

Several lines of research have explored simplified linear models as a means of studying and designing recurrent dynamics with greater interpretability. Continuous-time state-space models, such as those in [4], [5], have enabled efficient training of sequence models with long-range dependencies by leveraging structured state-space kernels. More recently, Muca et al. [6] provided a theoretical analysis of linear state-space models, clarifying their expressive power and the role of parameterization in controlling stability and memory retention. These models offer a valuable bridge between classical control theory and modern deep learning approaches to sequence modeling.

From a training dynamics perspective, Lee et al. [7] analyzed wide neural networks through the lens of the neural tangent kernel, providing insights into the coupling between parameters and outputs during optimization. Although this framework is often applied to feedforward networks, it has implications for understanding the parameter–state interaction in recurrent settings, particularly in regimes where network width and gating jointly influence effective learning rates. Complementary work by Saxe et al. [8] investigated exact learning dynamics in deep linear networks, showing how singular value spectra dictate time scales of parameter evolution. This resonates with our perspective that recurrent gates modulate effective time scales in both state and parameter spaces.

Another rich research area involves constraining recurrent weight matrices to improve stability, expressivity, or trainability. Orthogonal and unitary RNNs [9], [10], [11], [12], [13] maintain constant gradient norms over time, thus alleviating the vanishing/exploding gradient problem. Lipschitz RNNs [14] extend this idea by explicitly controlling the Lipschitz constant to ensure robustness. Non-normal RNNs [15] and their variants incorporating Schur decompositions [16] have been proposed to exploit transient amplification phenomena for richer dynamics. Other designs include antisymmetric RNNs [17], which draw inspiration from Hamiltonian systems to ensure stability, coupled RNNs [18], which model interacting subsystems, and multiscale RNNs [19], which embed explicit time-scale separation into the architecture. Related architectural innovations such as the Clockwork RNN [20] also demonstrate the utility of explicitly incorporating multiple time scales into recurrent dynamics.

Gating mechanisms have received particular attention for their role in modulating information flow and improving trainability. From a theoretical standpoint, [21] and [22] analyzed the effects of gating on dynamical isometry and mean-field properties in RNNs, showing that gates can help preserve gradient flow and condition the optimization landscape. Related analyses in feedforward networks [23] underline the generality of dynamical isometry principles across architectures. Architecturally, stacked gated RNNs [24] and hybrid designs such as the “Just Another Network” [25] demonstrate the versatility of gating in achieving both memory retention and

efficient optimization. More recent theoretical work further strengthens this connection: Krishnamurthy et al. [26] and Can et al. [27] showed that gates can create slow modes in recurrent dynamics, directly modulating Jacobian spectra and shaping effective memory time scales. Empirical studies such as [28] confirmed that RNNs tend to develop adaptive time scales when trained on multi-scale sequential data, further illustrating the deep connection between gating and temporal structure.

III. RNNs AND TIME-SCALES

We begin with a simple continuous-time RNN model [29]:

$$\frac{dx(t)}{dt} = \phi(W^r x(t) + W^i u(t)) - x(t), \quad x(0) = x_0, \quad (1)$$

where the state vector $x(t) \in \mathbb{R}^{N_r}$ evolves under the recurrent weights $W^r \in \mathbb{R}^{N_r \times N_r}$, input weights $W^i \in \mathbb{R}^{N_r \times N_i}$, and elementwise nonlinearity $\phi(\cdot)$.

The output is generated via a readout mapping

$$z(t) = \psi(x(t)), \quad (2)$$

which, in the common linear case, reduces to

$$z(t) = W^o x(t), \quad W^o \in \mathbb{R}^{N_o \times N_r}. \quad (3)$$

Different readout functions $\psi(\cdot)$ may be chosen depending on the task.

A. From continuous to discrete time

Applying a first-order Taylor expansion around t (i.e., Euler discretization) to (1) gives

$$x(t + \delta t) \approx x(t) + \delta t \frac{dx(t)}{dt}. \quad (4)$$

With unit step $\delta t = 1$, this yields the standard discrete-time RNN update

$$x_{t+1} = \phi(W^r x_t + W^i u_t). \quad (5)$$

B. Global time rescaling

Suppose we want to model a time-rescaled input $u(\alpha t)$ with (1). Let the state trajectory be reparameterized as $x(\alpha t)$ via a linear time-warping function

$$c(t) = \alpha t, \quad \alpha > 0. \quad (6)$$

Rewriting (1) with the new time variable, $T = c(t) = \alpha t$, we obtain:

$$\frac{dx(c(t))}{dt} = \frac{dx(T)}{dT} \frac{dT}{dt} = \alpha \phi(W^r x(t) + W^i u(t)) - \alpha x(t), \quad (7)$$

where we have renamed $t = T$ on the right-hand side to simplify the notation. This expression shows that a time-warping $c(t) = \alpha t$ scales both the recurrent and decay terms by the same factor α . Therefore, the original dynamics in (1) are *not* invariant under time-rescaling: the evolution is accelerated for $\alpha > 1$ and slowed down for $\alpha < 1$. In this sense, α acts as a global update rate, with $\alpha \rightarrow 0$ yielding nearly frozen dynamics and $\alpha \rightarrow \infty$ corresponding to very fast updates.

Discretizing (7) with (4) and $\delta t = 1$ yields

$$x_{t+1} = \alpha \phi(W^r x_t + W^i u_t) + (1 - \alpha)x_t, \quad (8)$$

which corresponds to *leaky integrator* neurons [30]. Here α is the *global state-update rate*, and its reciprocal $\tau = 1/\alpha \in [1, \infty)$ defines the global discrete-time scale. When $\alpha \rightarrow 0$, state updates occur very slowly, approaching a static memory.

C. General time warping and gating

To go beyond global rescaling and achieve invariance to more general time transformations, we allow an arbitrary monotonic, differentiable warping $c : \mathbb{R} \rightarrow \mathbb{R}$.

$$\begin{aligned} \frac{dx(c(t))}{dt} &= \frac{dc(t)}{dt} \phi(W^r x(t) + W^i u(t)) - \frac{dc(t)}{dt} x(t), \quad (9) \\ &= g(t) \phi(W^r x(t) + W^i u(t)) - g(t) x(t), \end{aligned}$$

where $g(t) := \frac{dc(t)}{dt}$ is the instantaneous state-update rate at time t . When $g(t) \equiv \alpha$, we recover the leaky case (7).

We parametrize $g(t)$ as a *gate*:

$$g(t) = \sigma(W^{r,g} x(t) + W^{i,g} u(t)), \quad (10)$$

where $\sigma(\cdot) \in (0, 1)$ is the logistic sigmoid, $W^{r,g} \in \mathbb{R}^{1 \times N_r}$, and $W^{i,g} \in \mathbb{R}^{1 \times N_i}$ are gate parameters. This parametrization ensures that the update rate $g(t)$ remains bounded in $(0, 1)$. Because $g(t)$ depends both on the current state $x(t)$ and the input $u(t)$, the effective time scale of the network becomes data- and state-dependent.

Discretizing (9) with $\delta t = 1$ gives

$$x_{t+1} = g_t \phi(W^r x_t + W^i u_t) + (1 - g_t) x_t, \quad (11)$$

which makes the dynamics invariant to a global rescaling of time via g_t .

For neuron-specific time scales, we assign an individual gate $g_t^{(j)}$ to each neuron j :

$$x_{t+1} = g_t \odot \phi(W^r x_t + W^i u_t) + (1 - g_t) \odot x_t, \quad (12)$$

where \odot denotes elementwise multiplication and $g_t \in (0, 1)^{N_r}$. Here $\sigma(\cdot)$ in (10) is applied componentwise, with $W^{r,g} \in \mathbb{R}^{N_r \times N_r}$ and $W^{i,g} \in \mathbb{R}^{N_r \times N_i}$. Each neuron thus possesses its own update rate (or time scale), enabling fine-grained adaptation of the network's temporal dynamics.

IV. BPTT-BASED TRAINING OF RNNs

A. Stochastic gradient descent in neural networks

The most basic form of the *stochastic gradient descent* (SGD) update rule for a parameter vector θ using a randomly sampled mini-batch of size $b \geq 1$ is

$$\theta_{l+1} = \theta_l - \frac{\mu}{b} \sum_{t=1}^b \frac{\partial \mathcal{E}_t}{\partial \theta_l}, \quad (13)$$

where l indexes the training iteration, $\mu > 0$ is the learning rate (or step size), and \mathcal{E}_t is the loss at sample t in the mini-batch. The stochasticity arises because each mini-batch is drawn at random from the training set, leading to noisy gradient estimates.

The gradient $\frac{\partial \mathcal{E}_t}{\partial \theta_l}$ in (13) can be expanded using the chain rule. For recurrent models, the dependence of the current state x_t on all previous states $\{x_k\}_{k < t}$ must be taken into account:

$$\sum_{t=1}^b \frac{\partial \mathcal{E}_t}{\partial \theta_l} = \sum_{t=1}^b \frac{\partial \mathcal{E}_t}{\partial x_t} \sum_{k=1}^t \frac{\partial x_t}{\partial x_k} \frac{\partial x_k}{\partial \theta_l}. \quad (14)$$

Here, the term $\frac{\partial x_t}{\partial x_k}$ is the product of Jacobian factors linking the state at time t to the state at time k , which makes the computation inherently sequential.

Because the gradients must be propagated backward through the sequence of states, this procedure is known as *backpropagation*. When applied to recurrent neural networks, where parameters are shared across time steps, the method is referred to as *backpropagation through time* (BPTT) [31].

B. Vanishing and exploding gradients

A central difficulty in computing (14) arises from the presence of long products of Jacobian matrices. For any $k < t$, the sensitivity of x_t with respect to x_k is given by

$$\frac{\partial x_t}{\partial x_k} = \prod_{j=k+1}^t J_j, \quad J_j = \frac{\partial x_j}{\partial x_{j-1}}, \quad (15)$$

where J_j is the Jacobian of the state update at time j .

Using the submultiplicative property of matrix norms, $\left\| \frac{\partial x_t}{\partial x_k} \right\| \leq \prod_{j=k+1}^t \|J_j\|$, and substituting into (14) gives the following upper bound on the gradient norm:

$$\left\| \frac{\partial \mathcal{E}_t}{\partial \theta_l} \right\| \leq \left\| \frac{\partial \mathcal{E}_t}{\partial x_t} \right\| \prod_{j=k+1}^t \|J_j\|. \quad (16)$$

Consider now the standard discrete-time RNN model (5). The Jacobian at step j has the form $J_j = D_{j-1} W^r$, where $D_j = \text{diag}(\phi'(a_j))$ is a diagonal matrix containing the derivatives of the activation function ϕ evaluated at the pre-activation $a_{j-1} = W^r x_{j-1} + W^i u_{j-1}$. The upper bound specializes to $\prod_{j=k+1}^t \|D_{j-1}\| \|W^r\|$. It is clear that if the spectral norm $\|W^r\|$ or the activation derivatives $\|D_{j-1}\|$ are consistently smaller than 1, the product will decay exponentially with $(t - k)$, leading to *vanishing gradients*. Conversely, if either factor is consistently greater than 1, the product will grow exponentially, producing *exploding gradients*. This spectral-norm dependence of the gradient magnitude is well documented in the literature [1] and motivates many of the stability constraints and reparameterizations used in modern RNN architectures.

V. HOW TIME-SCALES IN RNN STATES AFFECT PARAMETER DYNAMICS

In Section V-A, we derive the exact expressions for the Jacobian matrices associated with the RNN variants introduced in Section III. These Jacobians govern how perturbations to the hidden state propagate through time, and thus play a central role in both forward signal evolution and backward gradient flow. Building on these results, Section V-B analyzes how the time-scales embedded in the state-space dynamics interact with the optimization process. In particular, we show how the

presence of constant, scalar, or multiple gating mechanisms influences the effective learning rate and the direction of parameter updates, thereby shaping the behaviour of the gradient descent algorithm.

A. Jacobian matrices

1) *Leaky-integrator neurons*: For the leaky-integrator model (8), the Jacobian at time j is

$$J_j = \alpha D_{j-1} W^r + (1 - \alpha) I, \quad (17)$$

where I is the identity matrix and $D_{j-1} = \text{diag}(\phi'(a_{j-1}))$. Relative to the standard RNN Jacobian $D_{j-1} W^r$, the constant gate α scales the recurrent contribution while adding a skip connection proportional to $(1 - \alpha) I$, thereby tempering gradient decay or explosion.

2) *Single scalar gate*: Consider now the scalar-gated model (11). Defining the gate pre-activation $a_t^g = W^{r,g} x_t + W^{i,g} u_t$, $a_t^g \in \mathbb{R}$, the Jacobian becomes

$$\begin{aligned} J_j &= \left[\phi(a_{j-1}) \frac{\partial g_{j-1}}{\partial x_{j-1}} + g_{j-1} D_{j-1} W^r \right] \\ &+ \left[x_{j-1} \frac{\partial(1 - g_{j-1})}{\partial x_{j-1}} + (1 - g_{j-1}) I \right] \\ &= (\phi(a_{j-1}) - x_{j-1}) J_{j-1}^g + g_{j-1} D_{j-1} W^r + (1 - g_{j-1}) I \\ &= G_{j-1} + g_{j-1} D_{j-1} W^r + (1 - g_{j-1}) I, \end{aligned} \quad (18)$$

where

$$\begin{aligned} J_j^g &= \frac{\partial g_j}{\partial x_j} = \sigma'(a_j^g) W^{r,g}, & G_{j-1} &= d_{j-1} J_{j-1}^g, \\ d_{j-1} &= \phi(a_{j-1}) - x_{j-1}. \end{aligned} \quad (19)$$

Here $J_j^g \in \mathbb{R}^{1 \times N_r}$ and G_{j-1} is rank-1, being the outer product of d_{j-1} and J_{j-1}^g . Thus, the scalar gate introduces a low-rank correction G_{j-1} in addition to rescaling the recurrent and skip terms.

3) *Multiple gates*: For the multi-gated model (12), the gate pre-activation is a vector $a_j^g \in \mathbb{R}^{N_r}$, yielding the gate Jacobian

$$J_j^g = \frac{\partial g_j}{\partial x_j} = \text{diag}(\sigma'(a_j^g)) W^{r,g} = D_j^g W^{r,g}, \quad (20)$$

with $D_j^g = \text{diag}(\sigma'(a_j^g))$. In this case, $g_j \in \mathbb{R}^{N_r}$ is a vector of neuron-wise update rates.

Introducing the shorthand $\hat{d} = \text{diag}(d)$ for a diagonal matrix with vector d on the diagonal, and $\Gamma = \text{diag}(g)$, the Jacobian of the multi-gate RNN model reads

$$\begin{aligned} J_j &= \hat{\phi}(a_{j-1}) J_{j-1}^g + \Gamma_{j-1} D_{j-1} W^r - \hat{x}_{j-1} J_{j-1}^g + (I - \Gamma_{j-1}) \\ &= \hat{d}_{j-1} J_{j-1}^g + \Gamma_{j-1} D_{j-1} W^r + (I - \Gamma_{j-1}) \\ &= G_{j-1} + \Gamma_{j-1} D_{j-1} W^r + (I - \Gamma_{j-1}). \end{aligned} \quad (21)$$

Unlike the scalar case, here G_{j-1} is not rank-deficient, since it results from multiplying a diagonal matrix by a full matrix.

B. Time-scale coupling

In this section, we show that the interaction between state-space time scales and parameter updates gives rise to an *effective learning rate* μ^* , which generally differs from the nominal learning rate μ in (13). The precise form of μ^* depends on the chosen state-space model. To this end, without loss of generality we consider only one time-step t and expand the gradient formula in (14) as follows:

$$\frac{\partial \mathcal{E}_t}{\partial \theta_l} = \frac{\partial \mathcal{E}_t}{\partial x_t} \sum_{k=1}^t \left[\prod_{j=k+1}^t J_j \right] \frac{\partial x_k}{\partial \theta_l}. \quad (22)$$

1) *Constant gate case*: In the constant gate case $g_t \equiv \alpha \in (0, 1]$, the BPTT gradient can be written as

$$\frac{\partial E_t}{\partial \theta_l} = \frac{\partial E_t}{\partial x_t} \sum_{k=1}^t \left[\prod_{j=k+1}^t (I + \alpha A_{j-1}) \right] \frac{\partial x_k}{\partial \theta_l}. \quad (23)$$

where the Jacobian (17) is $J_j = I + \alpha A_{j-1}$, $A_{j-1} := D_{j-1} W_r - I$. Factoring α out of each Jacobian in the product gives

$$\begin{aligned} &\prod_{j=k+1}^t (I + \alpha A_{j-1}) \\ &= \left(\prod_{j=k+1}^t \alpha \right) \prod_{j=k+1}^t (\alpha^{-1} I + A_{j-1}) = \alpha^{t-k} \mathcal{P}_{t,k}, \end{aligned} \quad (24)$$

where we defined the normalized product $\mathcal{P}_{t,k} := \prod_{j=k+1}^t (\alpha^{-1} I + A_{j-1})$.

Substituting back, the gradient becomes

$$\frac{\partial E_t}{\partial \theta_l} = \frac{\partial E_t}{\partial x_t} \sum_{k=1}^t \alpha^{t-k} \mathcal{P}_{t,k} \frac{\partial x_k}{\partial \theta_l}. \quad (26)$$

The factor α^{t-k} is the exact multiplicative decay applied to gradient components that travel through $(t-k)$ recurrent steps. This means that gating induces a lag-dependent reweighting of gradient contributions, equivalent to a lag-dependent effective learning rate:

$$\mu_{t,k}^* = \mu \alpha^{t-k} + (\text{perturbative correction terms}). \quad (27)$$

Here the perturbative correction terms stem from the residual $(1 - \alpha) I$ contribution and from activation derivatives, which slightly distort the pure exponential decay. This makes explicit that the learning rate decays exponentially with temporal distance, at a rate mainly determined by α . For $\alpha < 1$, long-range dependencies are progressively downweighted, leading to a vanishing gradient phenomenon for long temporal distances.

2) *RNNs with scalar gate*: When considering the Jacobian in (18), the product of Jacobians inside the gradient update formula can be rewritten as:

$$\begin{aligned} &\prod_{j=k+1}^t G_{j-1} + g_{j-1} D_{j-1} W^r + (1 - g_{j-1}) I \\ &= \prod_{j=k+1}^t G_{j-1} + I + g_{j-1} (D_{j-1} W^r - I). \end{aligned} \quad (28)$$

The gradient equation becomes:

$$\begin{aligned} & \frac{\partial \mathcal{E}_t}{\partial \theta_l} \\ &= \frac{\partial \mathcal{E}_t}{\partial x_t} \sum_{k=1}^t \left[\prod_{j=k+1}^t G_{j-1} + I + g_{j-1}(D_{j-1}W^r - I) \right] \frac{\partial x_k}{\partial \theta_l}. \end{aligned} \quad (29)$$

In what follows, and in Section V-B3, we use the general first-order expansion from Appendix VIII-A, applied to products of Jacobian matrices with $\epsilon = 1$. Note that in the present setting the products correspond to BPTT Jacobian chains $\prod_{j=k+1}^t J_j$, which propagate sensitivities backward through time. Consequently, perturbation insertions appear between factors indexed by earlier and later time steps, but the ordering remains fully consistent with the general matrix product expansion derived in Appendix VIII-A.

Unlike the constant- α case, here the gate contributions cannot be factored out in closed form; the product involves time-varying, input-driven gates that interact with state dynamics. We rewrite each factor inside the product as

$$M_{j-1} = I + g_{j-1}A_{j-1} + G_{j-1}, \quad (30)$$

where $A_{j-1} = D_{j-1}W^r - I$ and G_{j-1} is a rank-1 matrix.

Expanding the matrix product (28) to the first order in the rank-1 corrections G_{j-1} , we obtain

$$\begin{aligned} \prod_{j=k+1}^t M_{j-1} &\approx \prod_{j=k+1}^t (I + g_{j-1}A_{j-1}) \\ &+ \sum_{m=k+1}^t \left(\prod_{j=m+1}^t (I + g_{j-1}A_{j-1}) \right) \\ &G_{m-1} \left(\prod_{j=k+1}^{m-1} (I + g_{j-1}A_{j-1}) \right). \end{aligned} \quad (31)$$

The first term describes the main dynamics without the rank-1 updates, while the second term is a sum of rank-1 perturbative corrections, each inserted at a different time step m and propagated by the main dynamics. These corrections remain small in practice because they arise from gate activation derivatives, whose range is inherently bounded by the saturating nature of the gating nonlinearity. We now factor the gate scalars g_{j-1} explicitly from the first term in (31) like we did in Section V-B1.

$$\begin{aligned} & \prod_{j=k+1}^t (I + g_{j-1}A_{j-1}) = \\ & \left(\prod_{j=k+1}^t g_{j-1} \right) \left(\prod_{j=k+1}^t (g_{j-1}^{-1}I + A_{j-1}) \right). \end{aligned} \quad (32)$$

Thus, the gate values contribute as a multiplicative attenuation factor given by the product $\prod_{j=k+1}^t g_{j-1}$, while the remaining matrices describe the dynamics normalized by g_{j-1} . Similarly, the rank-1 corrections remain rank-1 but acquire products of gates from the intervals before and after the insertion of G_{m-1} .

Collecting all terms, we can write

$$\begin{aligned} \prod_{j=k+1}^t M_{j-1} &\approx \left(\prod_{j=k+1}^t g_{j-1} \right) P_{t,k} \\ &+ \sum_{m=k+1}^t \left(\prod_{j=m+1}^t g_{j-1} \right) R_{t,m} G_{m-1} \left(\prod_{j=k+1}^{m-1} g_{j-1} \right) S_{k,m}, \end{aligned} \quad (33)$$

where $P_{t,k} = \prod_{j=k+1}^t (g_{j-1}^{-1}I + A_{j-1})$ and the normalized matrices are defined as $R_{t,m} = \prod_{j=m+1}^t (g_{j-1}^{-1}I + A_{j-1})$ and $S_{k,m} = \prod_{j=k+1}^{m-1} (g_{j-1}^{-1}I + A_{j-1})$.

Plugging (33) into the gradient expression, we obtain

$$\begin{aligned} \frac{\partial E_t}{\partial \theta_l} &= \frac{\partial E_t}{\partial x_t} \sum_{k=1}^t \left(\prod_{j=k+1}^t g_{j-1} \right) P_{t,k} \\ &+ \sum_{m=k+1}^t \left(\prod_{j=m+1}^t g_{j-1} \right) R_{t,m} \\ &G_{m-1} \left(\prod_{j=k+1}^{m-1} g_{j-1} \right) S_{k,m} \frac{\partial x_k}{\partial \theta_l}. \end{aligned} \quad (34)$$

Unlike the constant gate case, here the gates g_{j-1} are time-varying and driven by the input and state. Therefore, the attenuation factor is not a simple power (as with α), but a product of gate values along the time interval $[k+1, t]$. This product leads to the following effective learning rate:

$$\mu_{t,k}^* = \mu \prod_{j=k+1}^t g_{j-1} + (\text{perturbative correction terms}). \quad (35)$$

Here the perturbative correction terms arise from the residual $(1 - g_t)x_t$ pathway and from gate-gradient contributions. These introduce rank-1 modifications to the Jacobian products, modulating gradient propagation in a way that cannot be collapsed into a single scalar factor.

3) *RNNs with multiple gates*: When considering the Jacobian in (21) the gradient equation becomes:

$$\begin{aligned} & \frac{\partial \mathcal{E}_t}{\partial \theta_l} \\ &= \frac{\partial \mathcal{E}_t}{\partial x_t} \\ & \sum_{k=1}^t \left[\prod_{j=k+1}^t G_{j-1} + (\Gamma_{j-1}D_{j-1}W^r) + (I - \Gamma_{j-1}) \right] \frac{\partial x_k}{\partial \theta_l}. \end{aligned} \quad (36)$$

Each factor in the product appearing in the gradient expression reads

$$M_{j-1} = (I - \Gamma_{j-1}) + \Gamma_{j-1}A_{j-1} + G_{j-1}, \quad (37)$$

where $A_{j-1} = D_{j-1}W^r$, Γ_{j-1} is the diagonal matrix of neuron-specific gates and $G_{j-1} = \hat{d}_{j-1}J_{j-1}^g$ is a full-rank matrix in this case.

Unlike the scalar gate case, here Γ_{j-1} does not commute with A_{j-1} , and G_{j-1} is no longer rank-1. Therefore, the

factorization is more involved. We can rewrite in terms of perturbation as follows:

$$M_{j-1} = \Gamma_{j-1}(\tilde{A}_{j-1}) + G_{j-1}, \quad (38)$$

where $\tilde{A}_{j-1} = A_{j-1} + \Gamma_{j-1}^{-1}(I - \Gamma_{j-1})$, with $\Gamma_{j-1}^{-1}(I - \Gamma_{j-1})$ defined element-wise as $\text{diag}((1 - g_{j-1}^{(i)})/g_{j-1}^{(i)})$ for $g_{j-1}^{(i)} > 0$.

Similarly to the scalar gate case, we expand the product to first order in G_{j-1} :

$$\begin{aligned} \prod_{j=k+1}^t M_{j-1} &\approx \prod_{j=k+1}^t (\Gamma_{j-1} \tilde{A}_{j-1}) \\ &+ \sum_{m=k+1}^t \left(\prod_{j=m+1}^t \Gamma_{j-1} \tilde{A}_{j-1} \right) G_{m-1} \left(\prod_{j=k+1}^{m-1} \Gamma_{j-1} \tilde{A}_{j-1} \right). \end{aligned} \quad (39)$$

The first term describes the main dynamics through diagonal gates and normalized matrices \tilde{A}_{j-1} . The second term accounts for corrections due to G_{j-1} .

We now separate the diagonal gate products explicitly:

$$\prod_{j=k+1}^t (\Gamma_{j-1} \tilde{A}_{j-1}) = \left(\prod_{j=k+1}^t \Gamma_{j-1} \right) P_{t,k}, \quad (40)$$

where $P_{t,k} = \prod_{j=k+1}^t \tilde{A}_{j-1}$, and the product $\prod_{j=k+1}^t \Gamma_{j-1}$ is a diagonal matrix with entries $\left(\prod_{j=k+1}^t g_{j-1}^{(1)}, \dots, \prod_{j=k+1}^t g_{j-1}^{(N_r)} \right)$.

For the rank corrections, we define

$$R_{t,m} = \prod_{j=m+1}^t \tilde{A}_{j-1}, \quad S_{k,m} = \prod_{j=k+1}^{m-1} \tilde{A}_{j-1}.$$

The expansion to the first order becomes

$$\begin{aligned} \prod_{j=k+1}^t M_{j-1} &\approx \left(\prod_{j=k+1}^t \Gamma_{j-1} \right) P_{t,k} \\ &+ \sum_{m=k+1}^t \left(\prod_{j=m+1}^t \Gamma_{j-1} \right) R_{t,m} G_{m-1} \left(\prod_{j=k+1}^{m-1} \Gamma_{j-1} \right) S_{k,m}. \end{aligned} \quad (41)$$

Plugging (41) into the gradient formula, we obtain

$$\begin{aligned} \frac{\partial E_t}{\partial \theta_l} &= \frac{\partial E_t}{\partial x_t} \sum_{k=1}^t \left(\prod_{j=k+1}^t \Gamma_{j-1} \right) P_{t,k} \\ &+ \sum_{m=k+1}^t \left(\prod_{j=m+1}^t \Gamma_{j-1} \right) R_{t,m} \\ &G_{m-1} \left(\prod_{j=k+1}^{m-1} \Gamma_{j-1} \right) S_{k,m} \frac{\partial x_k}{\partial \theta_l}. \end{aligned} \quad (42)$$

Unlike the scalar gate case, here the gate contributions $\prod_{j=k+1}^t \Gamma_{j-1}$ form a *diagonal matrix* rather than a scalar. Consequently, the attenuation of the gradient is *neuron-specific* and depends on the entire input-driven gate trajectory:

$$\mu_{t,k}^{*(i)} = \mu \prod_{j=k+1}^t g_{j-1}^{(i)} + (\text{perturbative correction terms}), \quad (43)$$

where $\mu_{t,k}^{*(i)}$ is the effective learning rate associated with neuron i .

Here the perturbative correction terms involve interactions between gates and state updates, producing full-rank contributions that cannot be simplified into a scalar or diagonal factor. In the multi-gate case: (i) each neuron has its own time-varying effective learning rate determined by its specific gate trajectory; (ii) gradient propagation is substantially anisotropic: some directions may be damped strongly, while others may be preserved, depending on the distribution of gate trajectories across neurons; (iii) the correction terms act as neuron-coupling perturbations, making the effective scaling both magnitude- and direction-dependent.

VI. ANALOGIES BETWEEN GATING MECHANISMS AND ADAPTIVE GRADIENT DESCENT METHODS

We now turn to well-known variations of the basic gradient descent algorithm [32]. Our goal is to draw parallels between these algorithmic modifications and the implicit effects induced by tunable time-scales in RNN state dynamics. A summary is shown in Table I. In particular, we examine how gates – by shaping the Jacobian structure – alter the effective optimization behaviour of plain gradient descent, in ways reminiscent of learning rate schedules, momentum terms, or adaptive update rules.

The analysis in Sections V-B1–V-B3 shows that the Jacobian factors in gated RNNs naturally lead to multiplicative modulation of the backpropagated gradient. From the first-order expansion, this modulation directly translates into an effective learning rate that depends on the gate configuration.

a) Constant gate (α): In the constant-gate (leaky integrator) case, the gate value $\alpha \in (0, 1]$ is fixed throughout training and across all units. The dominant multiplicative factor in the backward product over $(t - k)$ steps is α^{t-k} , independent of the input sequence or hidden state trajectory. Unlike the time-varying or multi-gate cases, there is no data dependence: the scaling depends solely on $(t - k)$ and α , remaining fixed during training. This is analogous to a fixed preconditioning factor in gradient descent, where every parameter update is scaled by the same precomputed value.

b) Single time-varying gate (g_{j-1}): With a scalar gate g_{j-1} , the gradient is modulated by a global, input-driven attenuation factor that varies over time. This is conceptually similar to a learning rate schedule (e.g., exponential decay), with the key difference that the modulation emerges from the network's own state dynamics rather than from an externally prescribed schedule.

c) Multiple time-varying gates ($g_{j-1}^{(i)}$): In the multi-gate case, the modulation is neuron-specific, so each neuron i has its own effective learning rate, determined by the trajectory of its gate values. This mirrors adaptive optimizers such as Adam or RMSProp, which assign each parameter a distinct, dynamically adjusted step size.

d) Corrections due to G_{j-1} : The additional G_{j-1} terms, which arise naturally in the first-order expansion, introduce directional modifications to the gradient. In the single-gate case, these corrections are rank-1, acting as low-dimensional

perturbations akin to momentum. In the multi-gate case, G_{j-1} is full-rank, leading to anisotropic scaling reminiscent of the preconditioning performed by Adam and other second-order adaptive methods.

VII. SIMULATIONS

A. Effective learning rate induced by gates

We empirically verify that, even when SGD uses a fixed global step size μ , gating mechanisms induce a lag-dependent effective learning rate that depends on the state-space model. The central object we use is the lag-conditioned sensitivity, $S_{t,k} = \|M_{t,k}\|_2$, $M_{t,k} = \prod_{j=k+1}^t J_j$, whose magnitude reweights how much a gradient signal at time k influences the update due to a loss at time t . At each training checkpoint ℓ we aggregate these quantities to obtain an empirical effective learning rate profile. For every temporal distance $h = t - k$, we define

$$\tilde{\mu}_{\text{eff}}(h; \ell) \propto \text{median}_h S_{t,k}(\theta_\ell). \quad (44)$$

To ensure comparability across models and checkpoints, we report a normalized version anchored at unit lag:

$$\tilde{\mu}_{\text{eff}}(h; \ell) = \frac{\text{median}_h S_{t,k}(\theta_\ell)}{\text{median}_{h=1} S_{t,k}(\theta_\ell)}. \quad (45)$$

This construction emphasizes the relative attenuation with lag: all curves start from 1 at $h = 1$, so differences directly reflect how fast or slow the effective learning rate decays with temporal distance. The normalization removes global scale effects due to parameter growth and isolates the temporal structure of the effective learning rate.

a) Predictors and overlays: To interpret the empirical effective learning rates, we compare them against a simple *gate-product predictor* derived from the zeroth-order theory of Section V-B. For each model we define

$$P_{t,k}(\theta_\ell) = \begin{cases} \alpha^{t-k}, & \text{leaky (constant } \alpha), \\ \prod_{j=k+1}^t g_{j-1}, & \text{scalar gate,} \\ \frac{1}{N_r} \sum_{i=1}^{N_r} \prod_{j=k+1}^t g_j^{(i)}, & \text{multi-gate,} \end{cases} \quad (46)$$

which captures the multiplicative attenuation induced purely by the gates. We then form its lag-binned median

$$\bar{P}(h; \ell) = \text{median}_h P_{t,k}(\theta_\ell). \quad (47)$$

From this baseline predictor, we construct two reference curves to overlay on the empirical profiles:

$$\tilde{\mu}_{\text{pred}}^{(0)}(h; \ell) = \frac{\bar{P}(h; \ell)}{\bar{P}(1; \ell)}, \quad (\text{zeroth-order theory, no fitting}) \quad (48)$$

$$\tilde{\mu}_{\text{pred}}^{(\text{fit})}(h; \ell) = \left(\frac{\bar{P}(h; \ell)}{\bar{P}(1; \ell)} \right)^{s(\ell)}, \quad (\text{empirical correction}). \quad (49)$$

The first curve $\tilde{\mu}_{\text{pred}}^{(0)}$ is the direct theoretical prediction obtained by normalizing the gate-product decay. The second

curve $\tilde{\mu}_{\text{pred}}^{(\text{fit})}$ introduces a fitted exponent $s(\ell)$ that corrects for higher-order (perturbative) effects not captured by the pure gate product. The slope $s(\ell)$ is estimated at checkpoint ℓ via a robust log–log regression

$$\log S_{t,k} \approx a(\ell) + s(\ell) \log P_{t,k}, \quad (50)$$

restricted to the central predictor range (1%–99% quantiles) to avoid extreme-tail artifacts.

b) Interpretation of the slope: The slope provides a quantitative diagnostic of how gates renormalize effective learning rates:

- $s(\ell) = 0$: no lag dependence, i.e. the effective learning rate remains constant and equal to the nominal μ .
- $s(\ell) = 1$: exact agreement with the zeroth-order gate-product predictor, i.e. $\tilde{\mu}_{\text{eff}}(h) \propto P_{t,k}$.
- $s(\ell) > 1$: effective sensitivity decays more steeply with lag than the predictor, shortening the memory horizon and yielding more conservative updates.
- $0 < s(\ell) < 1$: effective sensitivity decays more slowly with lag than the predictor, extending the memory horizon and yielding more permissive updates.

c) Setup: We train each RNN model (leaky (8), scalar (11), multi-gate (12)) with plain SGD (no momentum, no adaptivity) on the adding problem. At selected checkpoints, we (i) run a fixed probe batch, (ii) build the exact one-step Jacobians J_j from Section V-A, (iii) estimate $S_{t,k}$ via a short power method iteration (5 steps) for $M_{t,k}$, a standard technique to approximate the largest singular value, (iv) compute $P_{t,k}$, and (v) produce the normalized lag profiles with theory overlays. We also track the fitted slope $s(\ell)$ across training. All reported quantities are averaged over 20 independent random seeds.

d) Results: Results are shown in Figures 3–5. Across all models, the empirical profiles $\tilde{\mu}_{\text{eff}}(h; \ell)$ exhibit a clear, monotone attenuation with lag and are well tracked by the fitted-power overlay $\tilde{\mu}_{\text{pred}}^{(\text{fit})}(h; \ell)$; the zeroth-order overlay $\tilde{\mu}_{\text{pred}}^{(0)}(h; \ell)$ captures the right trend but is consistently too aggressive, predicting faster decay than observed. The fitted log–log slopes extracted from the summaries (*slope*, R^2) are:

- **Leaky (constant α):** $s(\ell)$ remains approximately stable around 2.4 throughout training, with negligible variation from initialization to iteration 800 ($R^2 \approx 0.96$). The effective profile attenuates considerably more steeply than the pure α^h predictor, reflecting additional contraction from the perturbative terms (identity leakage and activation derivatives).
- **Scalar gate:** $s(\ell)$ starts at ≈ 0.45 at initialization and monotonically decreases to ≈ 0.31 by iteration 800 ($R^2 \approx 0.99$ throughout). The empirical profile decays more slowly than the product of gates, indicating that the $(1 - g_t)x_t$ pathway and gate-gradient terms partially counteract multiplicative attenuation, preserving longer-range contributions. The decreasing trend suggests that training progressively opens the gates, further mitigating attenuation.
- **Multi-gate:** $s(\ell)$ starts at ≈ 0.58 and increases slightly to ≈ 0.61 by iteration 800 ($R^2 \approx 0.99$). The attenuation is

TABLE I
CONCEPTUAL SIMILARITIES BETWEEN GATING-INDUCED GRADIENT MODULATION AND ADAPTIVE GRADIENT DESCENT METHODS.

Gating case	Gradient modulation	Analogy with optimizers
Constant gate (α)	Fixed scaling depending on distance ($t-k$)	SGD with a constant, precomputed scaling factor
Time-varying scalar gate (g_{j-1})	Global, input-driven scaling over time	SGD with a learning rate schedule
Multiple gates ($g_{j-1}^{(i)}$)	Per-neuron (diagonal) scaling	Adam/RMSProp (per-parameter adaptation)
Corrections (G_{j-1})	Directional modulation (rank-1 or full-rank)	Momentum / adaptive preconditioning

sublinear relative to the gate product but stronger than in the scalar case. While the multi-gate architecture implies neuron-wise anisotropy in principle (each unit has its own gate trajectory), our scalar sensitivity measure $S_{t,k}$ only captures the dominant contraction rate. The fitted slope $s(\ell)$ should therefore be interpreted as an aggregate effect of this anisotropic gating.

e) Takeaways: The fitted log-log slope $s(\ell)$ is never exactly 0 or 1, confirming two key aspects of our theory. First, since $s(\ell) \neq 0$, the empirical effective learning rate always diverges from the nominal learning rate, validating that gates structurally modulate optimization. Second, deviations from $s(\ell) = 1$ indicate the presence of first-order correction terms beyond the pure gate product. These corrections are not mere transient effects of optimization: $s(\ell)$ remains relatively stable across training, suggesting that the modulation is a structural property of the dynamics. At the same time, $s(\ell)$ is shaped by the task and data: problems that keep units in a near-linear regime with open gates yield $0 < s(\ell) < 1$ (slower-than-predictor decay), whereas tasks driving saturation or stronger filtering tend to produce $s(\ell) > 1$ (faster-than-predictor decay). In practice, the naive gate-product predictor is thus renormalized by first-order, task-dependent effects, so that observed deviations of $s(\ell)$ from unity quantify meaningful, problem-induced corrections to the effective learning rate.

B. Directional anisotropy: propagation vs. updates

Backpropagated signals in recurrent models are transported by Jacobian products $M_{t,k}$, which determine both how much gradient survives with lag (magnitude) and how it is distributed across directions (geometry). A concentrated singular spectrum of $M_{t,k}$ indicates that sensitivities align with a low-dimensional subspace in state space. However, parameter updates follow the realized gradients, which depend on the data and on how the loss projects onto these directions. To distinguish these two aspects, we report two complementary measurements:

(A) Propagation anisotropy (from Jacobians). For many (t, k) pairs with lag $h = t - k$, we compute the singular values $\sigma_1 \geq \sigma_2 \geq \dots$ of $M_{t,k}$ and summarize them with two indices. The *anisotropy index* (AI) measures spectral spread as the ratio of the largest to the r -th singular value, while the *cumulative energy* (CE) measures how much squared-singular-value mass

lies in the top- r subspace:

$$\text{AI}_r(M) = \text{median}_h \left(\frac{\sigma_1}{\sigma_r} \right), \quad (51)$$

$$\text{CE}_r(M) = \text{median}_h \left(\frac{\sum_{i=1}^r \sigma_i^2}{\sum_i \sigma_i^2} \right). \quad (52)$$

Medians are taken across (t, k) pairs with the same lag h to reduce sensitivity to extreme singular values that arise in long Jacobian products. An AI close to 1 indicates a nearly isotropic spectrum, while large values signal that a single direction dominates propagation; CE close to 1 indicates that most of the energy lies in the top- r directions.

(B) Parameter update anisotropy (from gradient covariance). We collect per-sample gradients into a matrix $G \in \mathbb{R}^{m \times p}$, where each of the m rows contains the flattened gradient of all p trainable parameters for one probe sequence. To isolate directional geometry, rows are ℓ_2 -normalized, columns are mean-centered, near-constant columns are removed, and a small jitter is added for numerical stability. The singular values of G are proportional to the square roots of the eigenvalues of the gradient covariance matrix $C = G^\top G$, so spectral analysis of G reveals the anisotropy of parameter update directions. If $\sigma_1 \geq \sigma_2 \geq \dots$ are the singular values of G , we report the same indices:

$$\text{AI}_r(G) = \frac{\sigma_1}{\sigma_r}, \quad \text{CE}_r(G) = \frac{\sum_{i=1}^r \sigma_i^2}{\sum_i \sigma_i^2}. \quad (53)$$

These metrics quantify how strongly parameter updates concentrate into a low-dimensional subspace under the training distribution.

a) Setup: We compare three models with the same state size: (i) plain RNN trained with Adam (no gates), (ii) scalar-gated RNN (11) trained with SGD, and (iii) multi-gated RNN (12) trained with SGD (per-neuron gates). We evaluate on five canonical sequence tasks: *adding*, *AR(2)*, *delay-sum*, *moving-average*, and *NARMA10*. For each task and model, we report AI/CE of Jacobian products vs. lag, and AI/CE from the gradient covariance. In all tasks, we use $r = 10, m = 256$ and train the models for 1200 iterations with no early stopping criterion. All reported quantities are averaged over 20 independent random seeds.

b) Results: A consistent picture emerges when comparing propagation anisotropy (from Jacobians) with parameter update anisotropy (from gradient covariances):

- **Jacobians.** Across all tasks, AIs rise steeply with lag and CE_{10} approaches 1, confirming that long-range transport of error signals is effectively low-dimensional. Strikingly, the plain RNN with Adam often exhibits the largest Jacobian AI at long lags (*adding*, *AR(2)*, *delay-sum*,

moving-average; cf. Figs. 6–10), largely because small singular values collapse at large h . For NARMA10, the same tendency holds, though by the final checkpoint the difference between Adam and gated models narrows.

- **Parameter updates.** Gradient-covariance analysis paints the opposite picture. Here, scalar and multi-gated models consistently dominate: $CE_{10}(G)$ sits in the 0.99–1.00 range for gates, versus 0.76–1.00 for plain+Adam; and $AI_{10}(G)$ is several times to more than an order of magnitude larger with gates on every task (adding: scalar/multi 18/26 vs. plain 5.4; AR(2): 19/20 vs. 5.7; delay-sum: 419/392 vs. 9.2; moving-average: 236/291 vs. 25; NARMA10: 491/703 vs. 10). Thus, while Adam appears highly anisotropic in terms of Jacobian transport, the actual update geometry excited by the loss concentrates much more strongly under gating.
- **Perturbative contributions.** The relative advantage of scalar vs. multi-gate depends on task structure. Multi-gate produces the strongest gradient-covariance anisotropy on most tasks, with the largest margin on nonlinear dynamics (NARMA10: 703 vs. 491) and temporal aggregation (moving-average: 291 vs. 236; adding: 26 vs. 18). The scalar gate is competitive on AR(2) (where both gates yield $AI \approx 19$ –20) and slightly exceeds multi-gate on delay-sum (419 vs. 392). This can be understood in light of the perturbative contributions derived in Equations (35) and (43): even though the leading-order effect of a scalar gate is rank-1, the correction terms vary with lag and can redirect sensitivity into different subspaces, inducing nontrivial gradient-covariance anisotropy. However, scalar gating is more fragile than neuron-wise gating in its directional control: on the adding task, the Jacobian CE_{10} collapses at the longest lags across the majority of seeds (cf. Figure 6), whereas multi-gate models preserve high CE_{10} even at large h , consistent with the stronger diagonal structure imposed by per-neuron gates.

c) Takeaways: All models develop low-dimensional propagation at long lags, but this can overstate the directional structure of updates. Jacobian spectra capture what the dynamics *could* amplify, whereas the gradient covariance reveals what optimization *actually* excites. Adam modifies the geometry of parameter updates but does not alter the state-space transport of gradients; in contrast, gating reshapes the recurrent dynamics themselves, so that realized gradients concentrate into coherent, low-dimensional subspaces of parameter space. Across all tasks, gated models induce markedly stronger update anisotropy than Adam, with near-total energy in the top- r directions. The relative advantage of per-neuron vs. scalar gating is task-dependent: multi-gate dominates on nonlinear or strongly interacting dynamics, while scalar gating can match or exceed it on specific linear tasks. Importantly, even scalar gating introduces perturbative contributions (cf. Eqs. (35), (43)), so that distinct lags can excite different directions and produce nontrivial gradient-covariance anisotropy despite the rank-1 leading order. For multi-gate models these contributions are full-rank, further enriching the spectrum of possible update directions.

C. Broader implications

The simulations of Sections VII-A and VII-B reveal that gating plays two complementary roles in recurrent learning dynamics: it modulates the magnitude of effective learning rates across lags (Section VII-A), and it shapes the directional structure of parameter updates through the geometry of Jacobian products and gradient covariance (Section VII-B).

From this perspective, gating acts as a structural prior on temporal credit assignment, biasing both the magnitude and geometry of gradient propagation. The relative advantage of scalar versus multi-gate architectures is task-dependent rather than following a simple complexity hierarchy: multi-gate models typically produce stronger gradient concentration, but scalar gating can match or even exceed this effect on certain tasks. Taken together, these results suggest that architectures and optimizers jointly determine not only how fast parameters move, but also which temporal and directional modes dominate learning.

VIII. CONCLUSIONS AND FUTURE DIRECTIONS

This work developed a unified dynamical systems theory of how gates in recurrent neural networks couple state evolution with parameter updates. We showed that gating mechanisms are not merely devices for controlling information flow in state space: they also act as implicit, data-driven preconditioners that modulate effective learning rates across lags and shape the directional geometry of gradient propagation. Through exact Jacobian derivations and first-order expansions, we made explicit how constant, scalar, and multi-dimensional gates induce adaptive step-size behavior, introduce anisotropy in parameter updates, and connect formally to classical optimization strategies such as learning-rate schedules, momentum, and Adam. These results position gating as a structural mechanism that embeds temporal geometry directly into the dynamics of learning, independent of any external optimizer.

The empirical simulations corroborate these theoretical insights across diverse synthetic sequence tasks. They confirm that gates systematically reshape both the magnitude and geometry of temporal credit assignment, producing low-dimensional update structure akin to—and in some cases stronger than—adaptive optimization methods.

More broadly, the analysis suggests that effective learning rates act as mesoscopic variables describing the coupling between fast state dynamics and slow parameter updates in recurrent networks. In the present work we focused on neuronwise effective learning rates, which capture how each unit retains and transmits temporal credit across lags. More refined descriptions could extend this framework to include between-neuron time scales describing how credit is transported across neurons through recurrent connectivity. Such extensions would complement the neuronwise picture developed here and may provide a richer account of how temporal credit assignment emerges from the interaction between architecture and optimization.

Future directions include extending this framework to LSTMs [33], GRUs [34], and transformers [35], as well as exploring hybrid strategies where gating and optimizer dynamics

are deliberately co-tuned to balance stability, efficiency, and representational power.

REFERENCES

- [1] R. Pascanu, T. Mikolov, and Y. Bengio, “On the difficulty of training recurrent neural networks,” in *Proceedings of the 30th International Conference on Machine Learning*, vol. 28, Atlanta, Georgia, USA, 2013, pp. 1310–1318.
- [2] N. Zucchet and A. Orvieto, “Recurrent neural networks: vanishing and exploding gradients are not the end of the story,” *Advances in Neural Information Processing Systems*, vol. 37, pp. 139402–139443, 2024.
- [3] A. Ceni, “Random orthogonal additive filters: A solution to the vanishing/exploding gradient of deep neural networks,” *IEEE Transactions on Neural Networks and Learning Systems*, vol. 36, no. 6, pp. 10794–10807, 2025.
- [4] A. Gu, K. Goel, and C. Ré, “Efficiently modeling long sequences with structured state spaces,” *arXiv preprint arXiv:2111.00396*, 2021.
- [5] A. Gu, I. Johnson, K. Goel, K. K. Saab, T. Dao, A. Rudra, and C. Ré, “Combining recurrent, convolutional, and continuous-time models with linear state space layers,” in *Thirty-Fifth Conference on Neural Information Processing Systems*, 2021.
- [6] N. Muca Cirone, A. Orvieto, B. Walker, C. Salvi, and T. Lyons, “Theoretical foundations of deep selective state-space models,” *Advances in Neural Information Processing Systems*, vol. 37, pp. 127226–127272, 2024.
- [7] J. Lee, L. Xiao, S. Schoenholz, Y. Bahri, R. Novak, J. Sohl-Dickstein, and J. Pennington, “Wide neural networks of any depth evolve as linear models under gradient descent,” *Advances in neural information processing systems*, vol. 32, 2019.
- [8] A. M. Saxe, J. L. McClelland, and S. Ganguli, “Exact solutions to the nonlinear dynamics of learning in deep linear neural networks,” *arXiv preprint arXiv:1312.6120*, 2013.
- [9] K. Helfrich, D. Willmott, and Q. Ye, “Orthogonal recurrent neural networks with scaled Cayley transform,” in *Proceedings of the 35th International Conference on Machine Learning*, ser. Proceedings of Machine Learning Research, J. Dy and A. Krause, Eds., vol. 80. PMLR, 10–15 Jul 2018, pp. 1969–1978.
- [10] Z. Mhammedi, A. Hellicar, A. Rahman, and J. Bailey, “Efficient orthogonal parametrisation of recurrent neural networks using householder reflections,” in *Proceedings of the 34th International Conference on Machine Learning*, 2017, p. 2401–2409.
- [11] M. Arjovsky, A. Shah, and Y. Bengio, “Unitary evolution recurrent neural networks,” in *International Conference on Machine Learning*, New York, USA, June 2016, pp. 1120–1128.
- [12] S. Wisdom, T. Powers, J. Hershey, J. Le Roux, and L. Atlas, “Full-capacity unitary recurrent neural networks,” in *Advances in Neural Information Processing Systems*, D. D. Lee, M. Sugiyama, U. V. Luxburg, I. Guyon, and R. Garnett, Eds. Barcelona, Spain: Curran Associates, Inc., Dec. 2016, pp. 4880–4888.
- [13] E. Vorontsov, C. Trabelsi, S. Kadoury, and C. Pal, “On orthogonality and learning recurrent networks with long term dependencies,” in *Proceedings of the 34th International Conference on Machine Learning*, 2017, p. 3570–3578.
- [14] N. B. Erichson, O. Azencot, A. Queiruga, L. Hodgkinson, and M. W. Mahoney, “Lipschitz recurrent neural networks,” *arXiv preprint arXiv:2006.12070*, 2021.
- [15] G. Kerg, K. Goyette, M. P. Touzel, G. Gidel, E. Vorontsov, Y. Bengio, and G. Lajoie, “Non-normal recurrent neural network (nnrmn): learning long time dependencies while improving expressivity with transient dynamics,” *arXiv preprint arXiv:1905.12080*, 2019.
- [16] A. Kag, Z. Zhang, and V. Saligrama, “RNNs incrementally evolving on an equilibrium manifold: A panacea for vanishing and exploding gradients?” in *International Conference on Learning Representations*, 2020.
- [17] B. Chang, M. Chen, E. Haber, and E. H. Chi, “AntisymmetricRNN: A dynamical system view on recurrent neural networks,” in *International Conference on Learning Representations*, 2019. [Online]. Available: <https://openreview.net/forum?id=ryxepo0cFX>
- [18] T. K. Rusch and S. Mishra, “Coupled oscillatory recurrent neural network (cornn): An accurate and (gradient) stable architecture for learning long time dependencies,” *ICLR*, 2021.
- [19] T. K. Rusch, S. Mishra, N. B. Erichson, and M. W. Mahoney, “Long expressive memory for sequence modeling,” *arXiv preprint arXiv:2110.04744*, 2021.
- [20] J. Koutnik, K. Greff, F. Gomez, and J. Schmidhuber, “A clockwork RNN,” in *International Conference on Machine Learning*, vol. 32, no. 2, 2014, pp. 1863–1871.
- [21] M. Chen, J. Pennington, and S. Schoenholz, “Dynamical isometry and a mean field theory of RNNs: Gating enables signal propagation in recurrent neural networks,” in *Proceedings of the 35th International Conference on Machine Learning*, ser. Proceedings of Machine Learning Research, J. Dy and A. Krause, Eds., vol. 80. Stockholm: PMLR, 10–15 Jul 2018, pp. 873–882.
- [22] D. Gilboa, B. Chang, M. Chen, G. Yang, S. S. Schoenholz, E. H. Chi, and J. Pennington, “Dynamical isometry and a mean field theory of lstms and grus,” *arXiv preprint arXiv:1901.08987*, 2019.
- [23] J. Pennington, S. Schoenholz, and S. Ganguli, “Resurrecting the sigmoid in deep learning through dynamical isometry: theory and practice,” in *Advances in Neural Information Processing Systems*, 2017, pp. 4785–4795.
- [24] M. O. Turkoglu, S. D’Aronco, J. D. Wegner, and K. Schindler, “Gating revisited: Deep multi-layer rnns that can be trained,” *IEEE Transactions on Pattern Analysis and Machine Intelligence*, vol. 44, no. 8, pp. 4081–4092, 2022.
- [25] J. Van Der Westhuizen and J. Lasenby, “The unreasonable effectiveness of the forget gate,” *arXiv preprint arXiv:1804.04849*, 2018.
- [26] K. Krishnamurthy, T. Can, and D. J. Schwab, “Theory of gating in recurrent neural networks,” *Physical Review X*, vol. 12, p. 011011, Jan 2022.
- [27] O. Can, K. Kapanova, and A. Sogaard, “Gates create slow modes in recurrent neural networks,” in *International Conference on Learning Representations (ICLR)*, 2020.
- [28] R. Quax, D. Kandhai, and P. M. A. Sloot, “Adaptive time scales in recurrent neural networks,” *Scientific Reports*, vol. 10, no. 1, p. 7442, 2020.
- [29] C. Tallec and Y. Ollivier, “Can recurrent neural networks warp time?” in *International Conference on Learning Representations*, 2018. [Online]. Available: <https://openreview.net/forum?id=SJcKhk-Ab>
- [30] H. Jaeger, M. Lukoševičius, D. Popovici, and U. Siewert, “Optimization and applications of echo state networks with leaky-integrator neurons,” *Neural Networks*, vol. 20, no. 3, pp. 335–352, 2007.
- [31] P. J. Werbos, “Backpropagation through time: what it does and how to do it,” *Proceedings of the IEEE*, vol. 78, no. 10, pp. 1550–1560, 1990.
- [32] S. Ruder, “An overview of gradient descent optimization algorithms,” *arXiv preprint arXiv:1609.04747*, 2016.
- [33] S. Hochreiter and J. Schmidhuber, “Long short-term memory,” *Neural Computation*, vol. 9, no. 8, pp. 1735–1780, 1997.
- [34] K. Cho, B. Van Merriënboer, C. Gulcehre, D. Bahdanau, F. Bougares, H. Schwenk, and Y. Bengio, “Learning phrase representations using RNN encoder-decoder for statistical machine translation,” *arXiv preprint arXiv:1406.1078*, 2014.
- [35] A. Vaswani, N. Shazeer, N. Parmar, J. Uszkoreit, Ł. Kaiser, and I. Polosukhin, “Attention is all you need,” in *Advances in Neural Information Processing Systems*, 2017.
- [36] N. J. Higham, *Functions of Matrices: Theory and Computation*. SIAM, 2008.
- [37] S. G. Krantz and H. R. Parks, *The Implicit Function Theorem: History, Theory, and Applications*. Boston, MA: Birkhäuser, 2003.
- [38] D. Kingma and J. Ba, “Adam: A method for stochastic optimization,” *arXiv preprint arXiv:1412.6980*, 2014.

SUPPLEMENTARY MATERIAL

A. Matrix product expansion via Fréchet derivatives

We derive here the first-order expansion of a product of matrices with structured perturbations, starting from the *product rule for the Fréchet derivative* (Theorem 3.3 in Higham [36]). We also show how the same reasoning naturally extends to higher-order terms.

1) *Fréchet differentiability and the first-order expansion*: Let $\mathbb{C}^{n \times n}$ denote the finite-dimensional vector space of complex $n \times n$ matrices equipped with a matrix norm (specifically, the operator 2-norm unless otherwise stated). Since the space is finite-dimensional, all norms are equivalent.

Definition VIII.1 (Fréchet differentiability [37], [36]). Let $f : \mathbb{C}^{n \times n} \rightarrow \mathbb{C}^{n \times n}$. We say that f is *Fréchet differentiable* at $A \in \mathbb{C}^{n \times n}$ if there exists a bounded linear mapping

$$L_f(A, \cdot) : \mathbb{C}^{n \times n} \rightarrow \mathbb{C}^{n \times n}$$

such that

$$\lim_{\|E\| \rightarrow 0} \frac{\|f(A+E) - f(A) - L_f(A, E)\|}{\|E\|} = 0. \quad (54)$$

The operator $L_f(A, \cdot)$ is called the *Fréchet derivative* of f at A , and it is unique if it exists.

a) *First-order expansion*.: If f is Fréchet differentiable at A , the first-order Taylor expansion reads

$$f(A+E) = f(A) + L_f(A, E) + o(\|E\|), \quad (55)$$

where $E \in \mathbb{C}^{n \times n}$ is the perturbation matrix specifying the direction and structure of the infinitesimal change applied to A . The notation $o(\|E\|)$ means that $\|o(\|E\|)\|/\|E\| \rightarrow 0$ as $\|E\| \rightarrow 0$.

b) *Product rule*.: If g and h are Fréchet differentiable at A , their product

$$f(X) = g(X)h(X)$$

satisfies the *product rule*

$$L_{gh}(A, E) = L_g(A, E)h(A) + g(A)L_h(A, E), \quad (56)$$

where $L_g(A, E)$ denotes the Fréchet derivative of g at A in the direction E ; see [36, Sec. 3.2, Thm. 3.3].

2) *Matrix products with structured perturbations*: Consider a product of n factors, each containing a perturbation proportional to a scalar parameter ε :

$$F(\varepsilon) = \prod_{j=1}^n (A_j + \varepsilon B_j), \quad (57)$$

where

- $A_j \in \mathbb{C}^{d \times d}$ is the unperturbed factor at position j ,
- $B_j \in \mathbb{C}^{d \times d}$ is the perturbation inserted at position j ,
- $\varepsilon \geq 0$ controls the magnitude of the perturbations.

The perturbation direction corresponds to the tuple

$$E = (B_1, B_2, \dots, B_n),$$

meaning that each factor in the product receives its own perturbation.

Since each factor in (57) is affine in ε , the function $F(\varepsilon)$ is a polynomial in ε of degree at most n .

3) *Recursive application of the product rule*: For any $k \leq n$ define

$$F_k(\varepsilon) := \prod_{j=1}^k (A_j + \varepsilon B_j), \quad F_n(\varepsilon) = F_{n-1}(\varepsilon)(A_n + \varepsilon B_n).$$

Apply the product rule (56) to F_n with

$$g(\varepsilon) = F_{n-1}(\varepsilon), \quad h(\varepsilon) = A_n + \varepsilon B_n.$$

At $\varepsilon = 0$ we have

$$g(0) = F_{n-1}(0) = A_1 A_2 \cdots A_{n-1}, \quad h(0) = A_n, \quad L_h(0, E) = B_n.$$

The product rule gives

$$L_{F_n}(0, E) = L_g(0, E)A_n + (A_1 \cdots A_{n-1})B_n. \quad (58)$$

- The first term propagates the derivative into the earlier factors.

- The second term inserts the perturbation B_n in the last position.

Iterating this recursion yields the general expression

$$L_{F_n}(0, E) = \sum_{i=1}^n \left(\prod_{j=1}^{i-1} A_j \right) B_i \left(\prod_{j=i+1}^n A_j \right), \quad (59)$$

where empty products are interpreted as the identity matrix.

a) *Illustration for $n = 3$.* Write

$$F_3(\varepsilon) = (A_1 + \varepsilon B_1)(A_2 + \varepsilon B_2)(A_3 + \varepsilon B_3).$$

Applying the recursive expansion gives

$$L_{F_3}(0, E) = B_1 A_2 A_3 + A_1 B_2 A_3 + A_1 A_2 B_3.$$

Each term contains exactly one perturbation B_i inserted at position i .

4) *First-order expansion of the matrix product:* Applying the Taylor expansion (55) to (57) gives

$$F(\varepsilon) = F(0) + \varepsilon L_F(0, E) + O(\varepsilon^2), \quad (60)$$

where $F(0) = \prod_{j=1}^n A_j$ and $L_F(0, E)$ is given by (59). Substituting yields

$$F(\varepsilon) = \underbrace{\left(\prod_{j=1}^n A_j \right)}_{\text{dominant dynamics}} + \varepsilon \underbrace{\sum_{m=1}^n \left(\prod_{j=1}^{m-1} A_j \right) B_m \left(\prod_{j=m+1}^n A_j \right)}_{\text{perturbative correction terms}} + O(\varepsilon^2). \quad (61)$$

a) *Higher-order terms:* The same combinatorial structure extends to higher derivatives. Since each factor $(A_j + \varepsilon B_j)$ is affine in ε , the expansion terminates at order n .

The r -th derivative of $F(\varepsilon)$ at $\varepsilon = 0$ is

$$F^{(r)}(0) = r! \sum_{1 \leq m_1 < \dots < m_r \leq n} \left(\prod_{j=1}^{m_1-1} A_j \right) B_{m_1} \left(\prod_{j=m_1+1}^{m_2-1} A_j \right) B_{m_2} \dots B_{m_r} \left(\prod_{j=m_r+1}^n A_j \right), \quad (62)$$

where empty products denote the identity matrix.

Consequently,

$$F(\varepsilon) = \sum_{r=0}^n \frac{\varepsilon^r}{r!} F^{(r)}(0). \quad (63)$$

For $r = 1$, Eq. (62) reduces to the first derivative

$$F^{(1)}(0) = L_F(0, E)$$

appearing in Eq. (61). Higher-order terms correspond to simultaneous perturbations inserted at multiple positions in the product.

B. Simulations supporting the validity of the first-order approximation

The perturbative analysis relies on the matrix product expansion derived in Appendix VIII-A. In that formulation, the Jacobian factors are decomposed as

$$M_j = A_j + \varepsilon B_j,$$

where A_j represents the dominant component of the Jacobian and B_j corresponds to gate-induced corrections. The product

$$F(\varepsilon) = \prod_{j=1}^n (A_j + \varepsilon B_j)$$

admits the first-order approximation

$$T_1(\varepsilon) = F(0) + \varepsilon L_F(0, B),$$

where $L_F(0, B)$ denotes the Fréchet derivative of the product (Appendix VIII-A). The approximation is accurate when the perturbative terms $\|B_j\|$ are small relative to $\|A_j\|$, so that the neglected $O(\varepsilon^2)$ contributions remain negligible.

We validate the expansion on a synthetic multi-frequency sinusoidal input signal: each input channel is a slowly varying sinusoid with a distinct frequency, plus a small amount of Gaussian noise. This choice is deliberate: the smooth, bounded nature of the signal keeps the gate pre-activations in a moderate regime where the sigmoid nonlinearity is neither saturated

nor near-linear, producing gate values that are genuinely time-varying while remaining well-conditioned. This ensures that the perturbative matrices B_j are non-trivial—i.e., the gates are actively modulating the dynamics—yet remain small relative to the dominant matrices A_j , which is precisely the regime where the first-order expansion is expected to be accurate. Using a task-specific training signal (such as the adding problem) would conflate two effects—the validity of the expansion and the particular optimization trajectory—whereas the synthetic signal isolates the geometric question of whether the Jacobian factorization satisfies the perturbative regime.

To empirically verify that this regime holds for the RNN models considered in the paper, we evaluate two complementary diagnostics. It is important to note that the first-order approximation is not expected to hold uniformly for arbitrary RNN architectures or tasks, since the relative magnitude of the perturbative terms B_j depends on the operating regime of the network and the statistics of the input sequence. The purpose of the following analysis is therefore not to establish a universal property of gated RNNs, but rather to verify that the perturbative assumptions underlying the theoretical analysis are satisfied in the specific experimental settings studied in this work.

First, for a range of ε values we measure the truncation error

$$E_{\text{trunc}}(\varepsilon) = \|F(\varepsilon) - T_1(\varepsilon)\|.$$

If the perturbative expansion is valid, the truncation error should scale as $O(\varepsilon^2)$. To visualize this behaviour we also report the normalized remainder

$$C_2(\varepsilon) = \frac{E_{\text{trunc}}(\varepsilon)}{\varepsilon^2},$$

which should approach a constant as $\varepsilon \rightarrow 0$.

Second, in the operating regime of the paper ($\varepsilon = 1$), we evaluate the relative magnitude of the perturbative matrices by measuring the per-step operator-norm ratio

$$r_j = \frac{\|B_j\|_2}{\|A_j\|_2}.$$

Small values of r_j indicate that the perturbative terms remain substantially smaller than the dominant Jacobian contributions, ensuring that higher-order corrections remain negligible.

All reported diagnostics are averaged over 20 independent random seeds in order to mitigate variability due to random initialization and stochastic training dynamics.

a) Scalar-gate model: Figure 1 reports these diagnostics for the scalar-gated RNN. The truncation error (top-left panel) follows a clear ε^2 scaling across the full range up to $\varepsilon = 1$, confirming the second-order accuracy of the first-order expansion. The normalized remainder $C_2(\varepsilon)$ (top-right panel) stabilizes to a constant as ε decreases, consistent with the dominant residual being exactly quadratic. Although the interquartile range appears visually broad due to the scale of the plot, the absolute spread remains numerically modest, confirming that $C_2(\varepsilon)$ is well confined around a stable value across random seeds. The bottom panels examine the perturbative matrices: the per-step norms $\|B_j\|_2$ remain consistently smaller than $\|A_j\|_2$ (bottom-left), and the ratio distribution r_j (bottom-right) is concentrated below 0.1, confirming that the gate-induced corrections are a minor perturbation of the dominant dynamics.

b) Multi-gate model: Figure 2 shows the analogous diagnostics for the multi-gated RNN. The same ε^2 scaling of the truncation error is observed, and $C_2(\varepsilon)$ again converges to a constant, albeit at a slightly higher plateau than in the scalar case. The ratio r_j is even more tightly concentrated at small values, reflecting the additional structure of the multi-gate parameterization. Overall, both architectures comfortably satisfy the perturbative regime assumed by the first-order expansion.

C. Scope and limitations of the first-order approximation

The goal of the first-order expansion in Appendix VIII-A is not to provide an exact description of the full Jacobian product dynamics, but rather to make explicit how gating mechanisms couple state-space time-scales with parameter updates during training. By isolating the leading-order contributions of the Jacobian factors, the expansion reveals how gate values modulate the magnitude and direction of gradient propagation. In particular, the analysis highlights the emergence of neuronwise effective learning rates, which act as mesoscopic variables describing how temporal credit assignment is modulated across recurrent steps.

Focusing on neuronwise contributions is meaningful when the dominant effect of gating is to modulate the diagonal structure of the Jacobian factors. In this regime, the gate products capture the main attenuation of gradients associated with each neuron. The simulations reported in Section VIII-B support this interpretation: the perturbative matrices B_j remain consistently small relative to the dominant matrices A_j , and the truncation error follows the expected $O(\varepsilon^2)$ scaling. These empirical results indicate that, for the tasks and architectures considered here, the first-order expansion captures the principal mechanism by which gating shapes effective learning rates.

At the same time, this approximation is not expected to hold uniformly across all regimes of recurrent learning. In particular, the perturbative assumption may break down when off-diagonal interactions dominate the Jacobian structure. A simple example arises when strong recurrent mixing causes gradient transport to propagate across many neurons before returning to the original

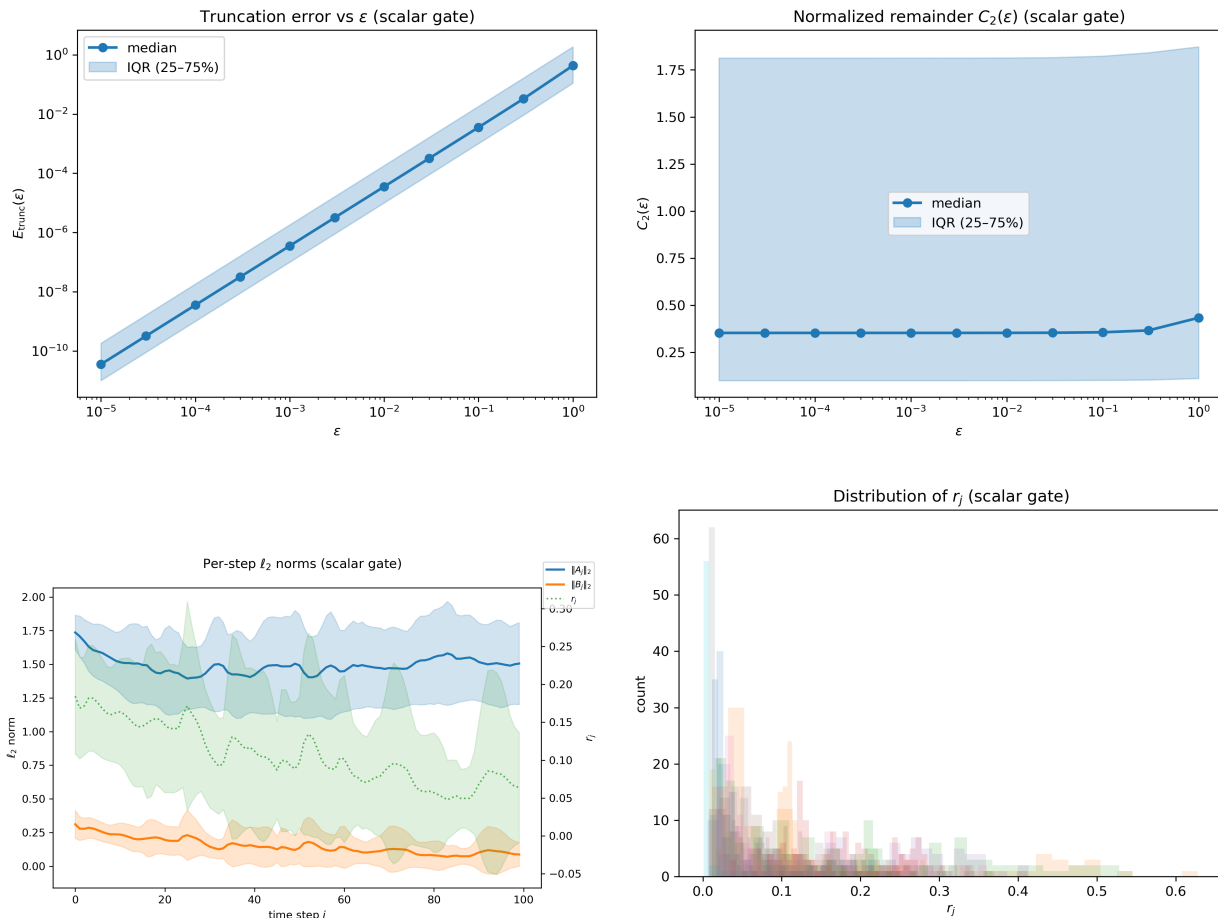


Fig. 1. Scalar-gated RNN. Top: truncation error versus ϵ (left) and normalized remainder $C_2(\epsilon)$ (right). Bottom: per-step norms $\|A_j\|_2$ and $\|B_j\|_2$ (left) and distribution of ratios r_j (right).

coordinate. In such cases, higher-order terms in the matrix product expansion can accumulate and significantly alter the effective gradient dynamics. Similarly, regimes involving highly nonlinear state trajectories or strongly saturated gates may produce correction terms that are no longer negligible relative to the dominant dynamics.

These limitations should not be viewed as shortcomings of the approach, but rather as indications of the level of description targeted by the present analysis. The first-order expansion provides a mathematically tractable framework for isolating neuronwise time-scales and revealing their role in the coupling between state dynamics and parameter updates. More refined descriptions are possible by extending the perturbative framework to include higher-order terms or by explicitly modeling off-diagonal transport effects. Such extensions would naturally lead to the notion of *between-neuron time-scales*, in which credit assignment is described not only by neuronwise retention but also by transport processes across neurons.

From this perspective, the first-order expansion should be interpreted as the leading-order component of a broader hierarchy of models describing temporal credit assignment. The present work focuses on the neuronwise level of this hierarchy, while more complex descriptions—including inter-neuron transport mechanisms—remain an interesting direction for future investigation.

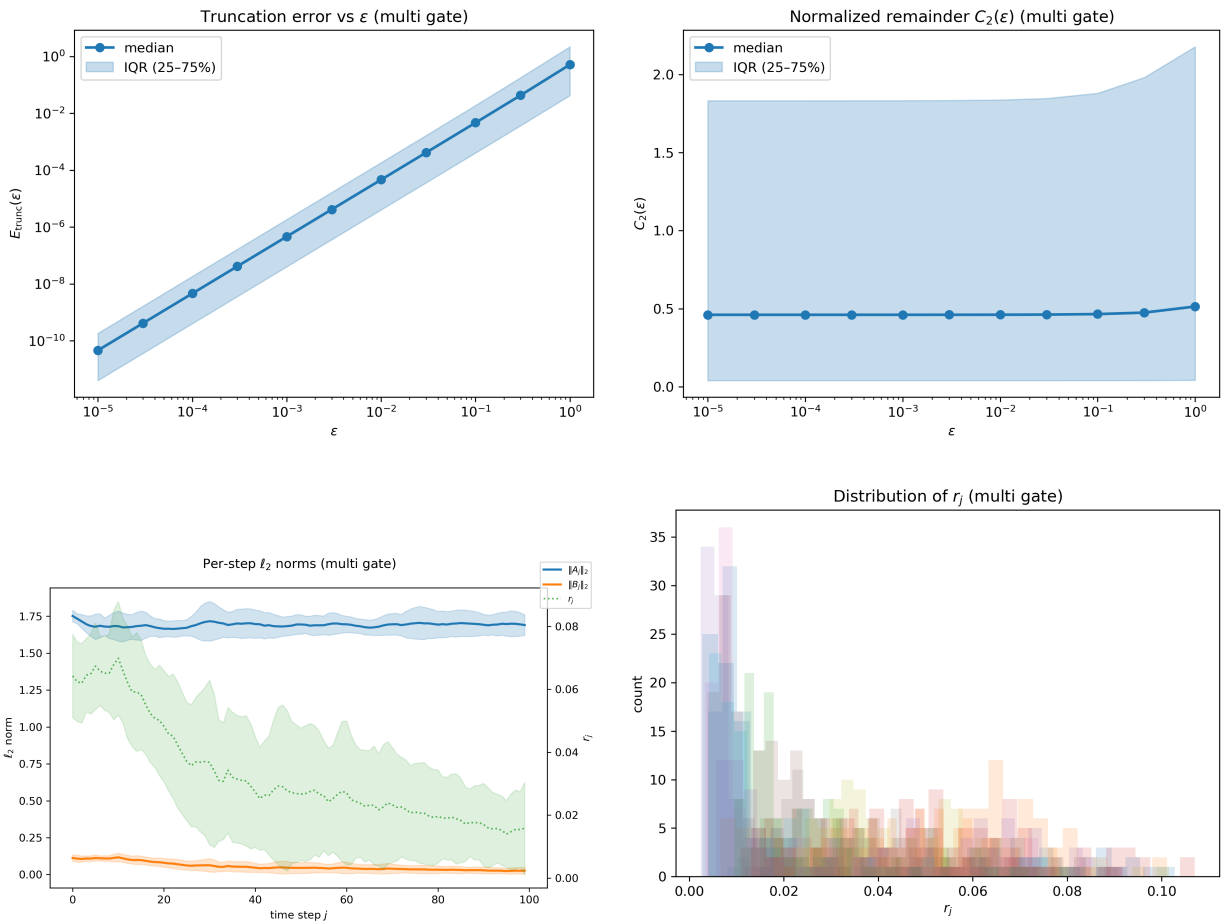


Fig. 2. Multi-gated RNN. Top: truncation error versus ε (left) and normalized remainder $C_2(\varepsilon)$ (right). Bottom: per-step norms $\|A_j\|_2$ and $\|B_j\|_2$ (left) and distribution of ratios r_j (right).

D. Adam

Adam [38] combines ideas from momentum methods and adaptive learning rate algorithms. Like Adadelta and RMSprop, it maintains an exponentially decaying average of past squared gradients $v_{t,l}$, but it also tracks an exponentially decaying average of past (unsquared) gradients $m_{t,l}$, akin to momentum:

$$m_{t,l} = \beta_1 m_{t,l-1} + (1 - \beta_1) \frac{\partial \mathcal{E}_t}{\partial \theta_l}, \quad (64)$$

$$v_{t,l} = \beta_2 v_{t,l-1} + (1 - \beta_2) \left(\frac{\partial \mathcal{E}_t}{\partial \theta_l} \right)^2, \quad (65)$$

where $\beta_1, \beta_2 \in (0, 1)$ are decay rates, and the squaring in $v_{t,l}$ is applied component-wise.

To correct the initialization bias introduced by these moving averages, Adam computes bias-corrected estimates:

$$\hat{m}_{t,l} = \frac{m_{t,l}}{1 - \beta_1^l}, \quad (66)$$

$$\hat{v}_{t,l} = \frac{v_{t,l}}{1 - \beta_2^l}. \quad (67)$$

The parameter update is then:

$$\theta_{l+1} = \theta_l - \frac{\mu}{b} \sum_{t=1}^b \frac{\hat{m}_{t,l}}{\sqrt{\hat{v}_{t,l} + \epsilon}}, \quad \epsilon > 0, \quad (68)$$

where b is the mini-batch size and ϵ is a small constant to prevent division by zero.

E. Figures of the simulations

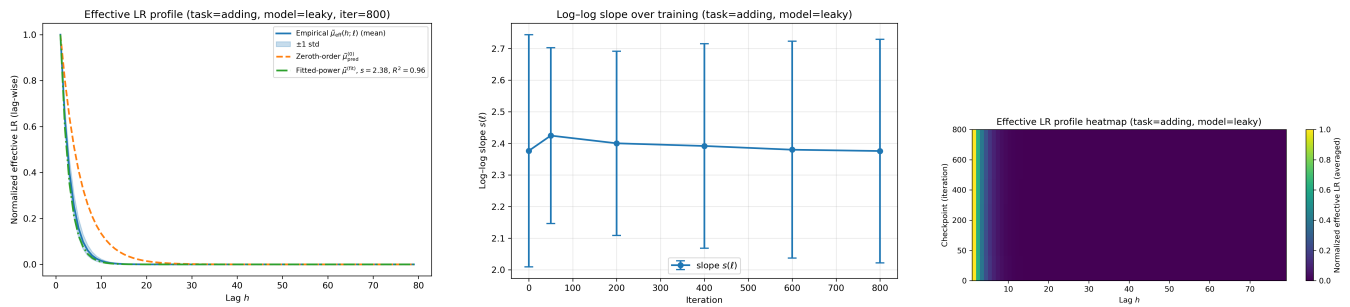


Fig. 3. Leaky RNN (constant α): normalized effective LR profile at final checkpoint (left), slope $s(\ell)$ across iterations (middle), and full sensitivity heatmap(right).

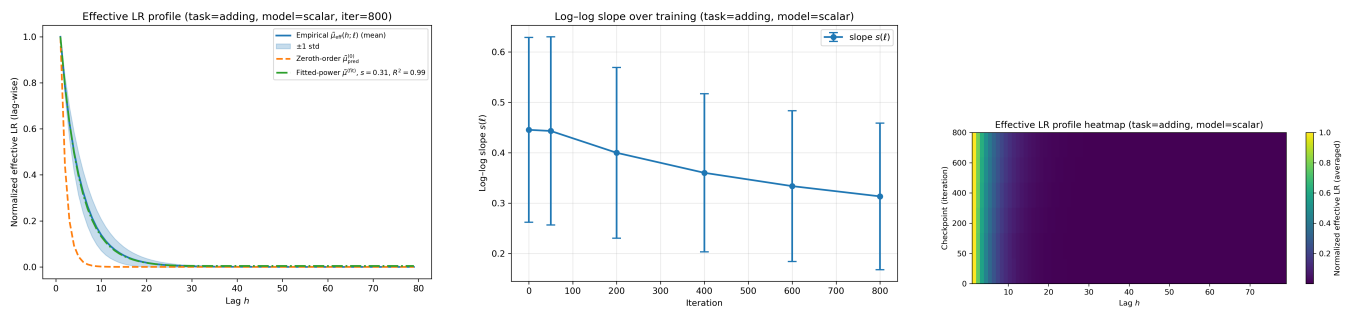


Fig. 4. Scalar-gated RNN: normalized effective LR profile at final checkpoint (left), slope $s(\ell)$ across iterations (middle), and full sensitivity heatmap (right).

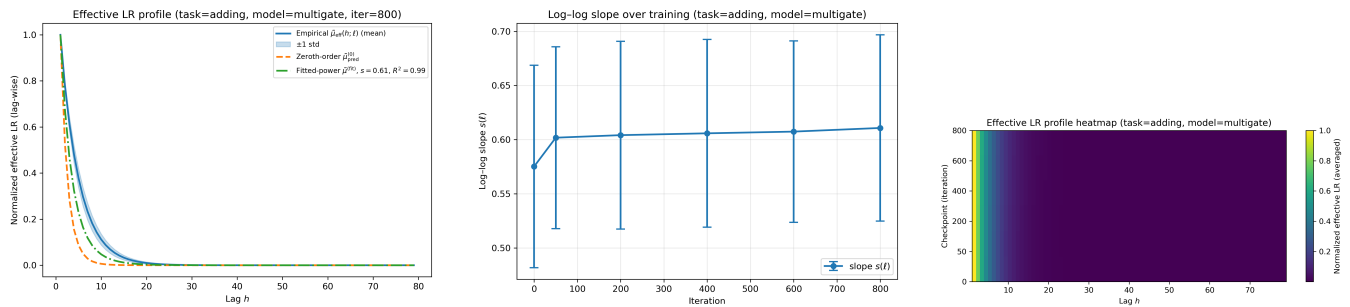


Fig. 5. Multi-gated RNN: normalized effective LR profile at final checkpoint (left), slope $s(\ell)$ across iterations (middle), and full sensitivity heatmap (right).

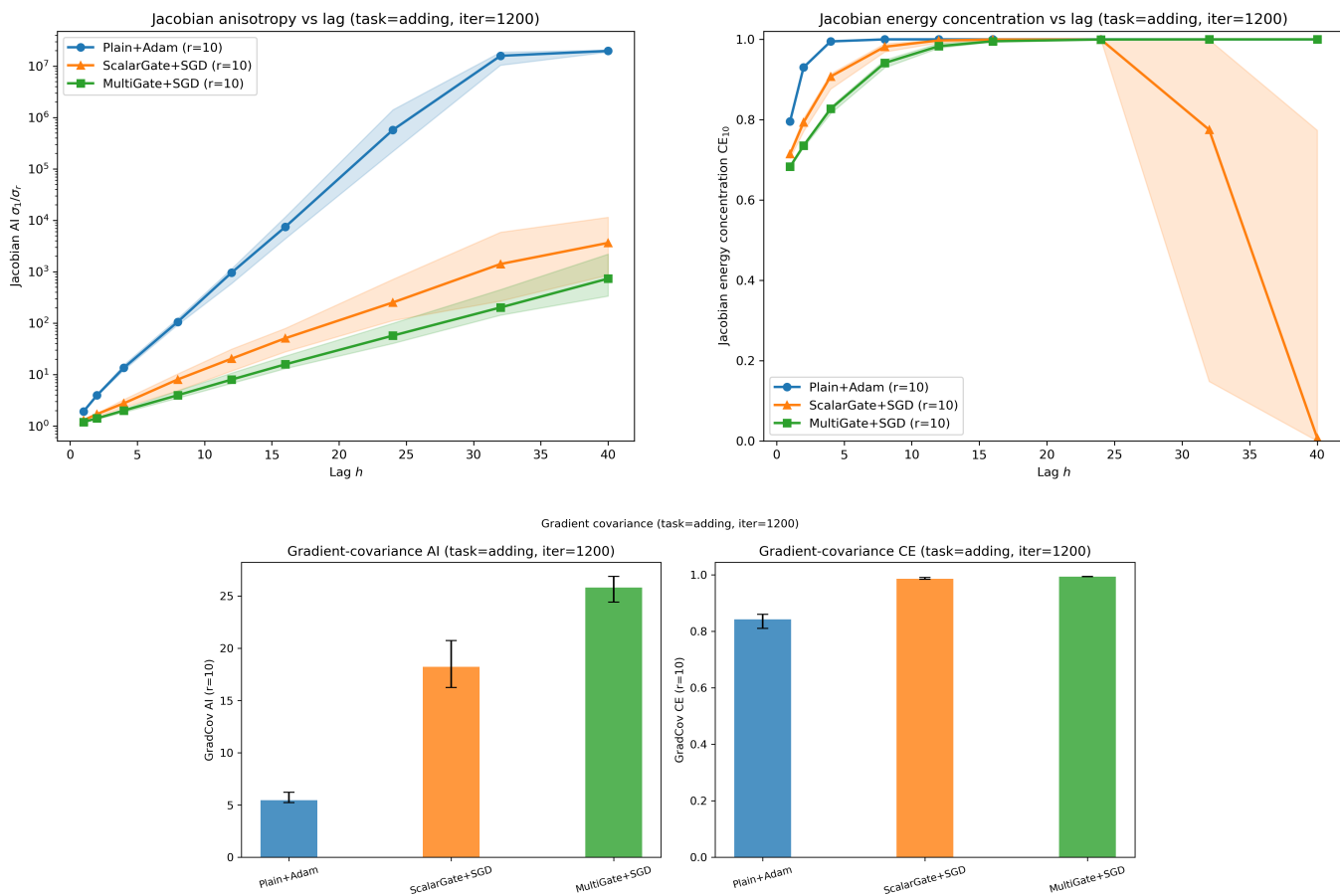


Fig. 6. Adding task. Left/middle: propagation anisotropy (AI, CE) vs. lag. Bottom: update anisotropy from gradient covariance (higher is more concentrated).

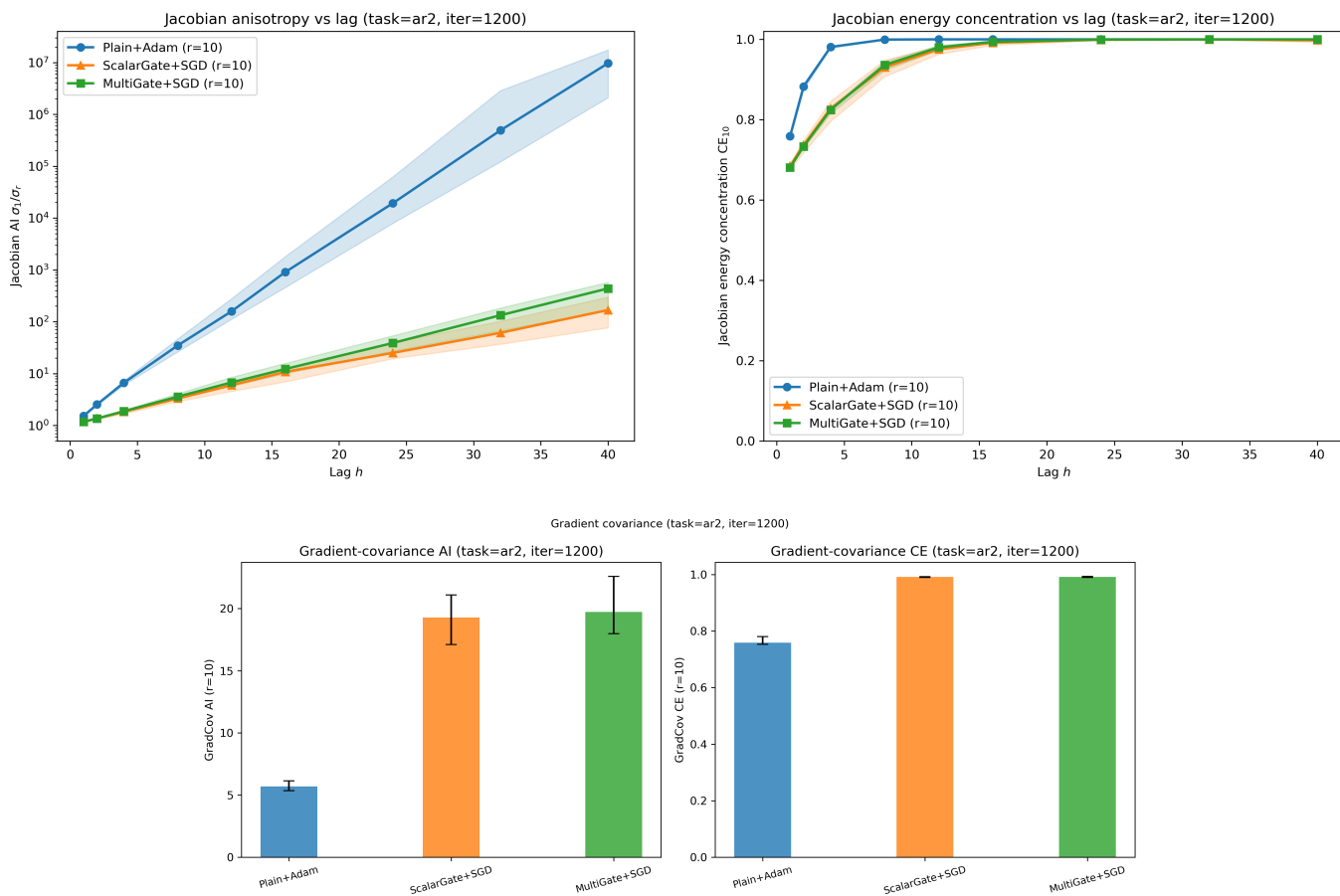


Fig. 7. AR(2). Propagation is highly anisotropic for all models; updates concentrate much more with gates.

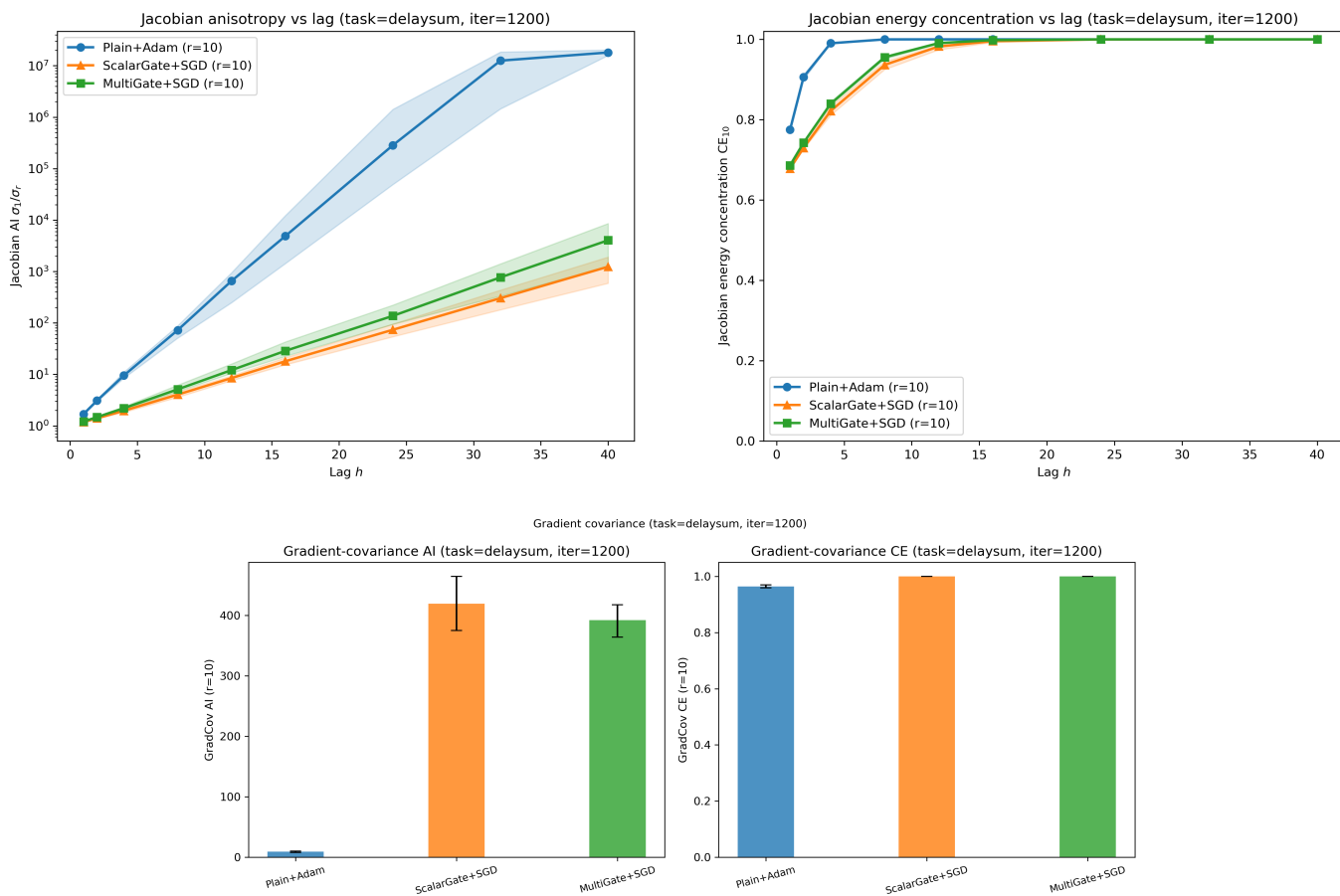


Fig. 8. Delay-sum. Update anisotropy is extreme for scalar/multi gates; Adam remains much flatter.

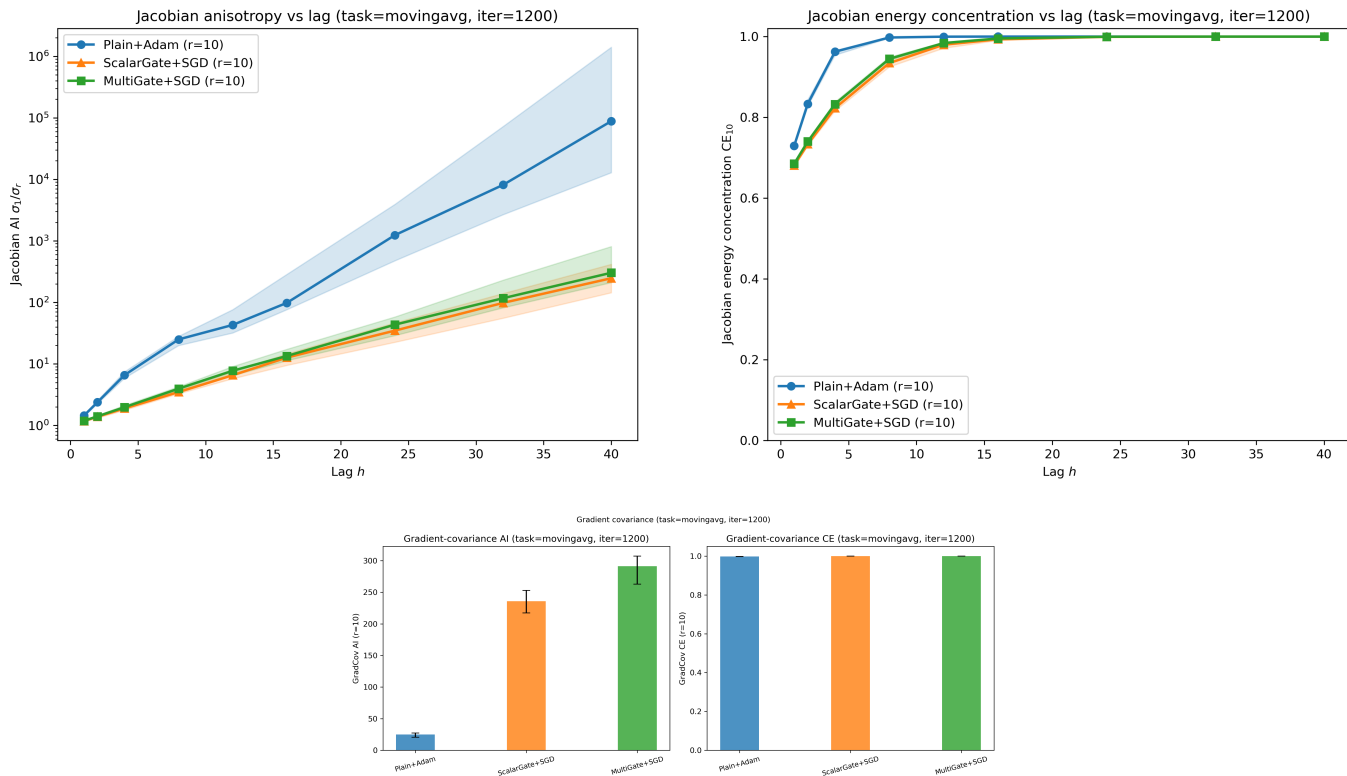


Fig. 9. Moving-average. Multi-gate shows the strongest update concentration; scalar is a close second.

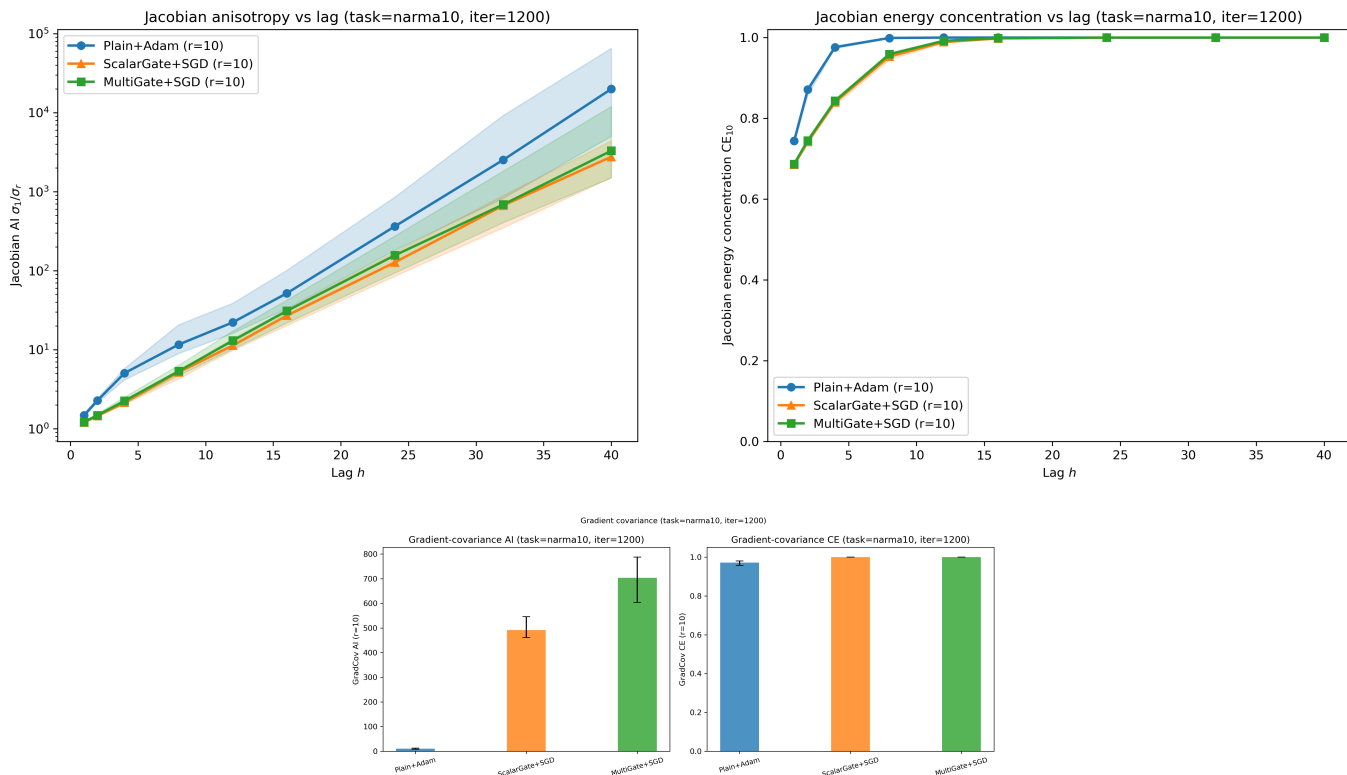


Fig. 10. NARMA10. The gap between gated and Adam models is largest in update anisotropy.

F. Code availability

The code used to reproduce the experiments reported in this paper is available at

<https://github.com/lorenzolivi/effective-learning-rates>

The repository includes scripts and instructions for reproducing the results.